TÉCNICO LISBOA

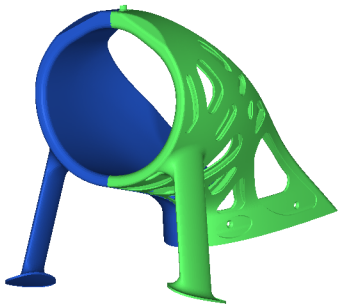

# Numeric Optimization of Metallic Component With Deformation in the Plastic Regime

**Hugo Jorge Gonçalves Marques**

Thesis to obtain the Master of Science Degree in

## Aerospace Engineering

Supervisors: Prof. Luís Alberto Gonçalves de Sousa
Profª Maria Alexandra dos Santos Gonçalves de Aguiar Gomes

## Examination Commitee

Chairperson: Prof. Fernando José Parracho Lau
Supervisor: Prof. Luís Alberto Gonçalves de Sousa
Members of the Commitee: Prof. José Arnaldo Pereira Leite Miranda Guedes

**July 2014**

À minha família, que me ajudou a chegar aqui

# Acknowledgments

This work would not be possible without the agreement and consent of both the company Optimal Structural Solutions lda and the Scientific Center of Aeronautic and Aerospace Technologies of the Superior Technical Institute (IST). For this reason, I would like to express my deepest appreciation to both, for allowing me the creation of this work.

A very special thank you goes in particular to this work technical supervisor António Reis from Optimal, and guiding teacher Alexandra Gomes from IST. Both were, and are, an inspirational source to me, and helped me motivating.

To professor André Marta, for having voluntarily created a master thesis latex template available for all students, I would like to express my deepest appreciation for sparring so many students precious hours of hard work, and accelerating the process of learning the code.

At last but not least, I here register my infinite gratitude to my beloved family and friends that encouraged me to do this work, regardless of the sacrifices that meant.

# Resumo

Neste trabalho realizou-se uma optimização topológica, com o objectivo de minimizar peso, a um componente metálico que sofre deformações plásticas de material. A optimização topológica é feita combinando o uso de códigos comerciais com optimização manual.

Este componente é carreado por um punção circular. Por este motivo, é modelada uma análise de contacto. As deformações durante a fase de carga são consideráveis e é ultrapassado o regime linear elástico do material; por este motivo, são também realizadas análises geometricamente não lineares com materiais não lineares com o recurso a códigos comerciais.

Dado que se trata de um componente importante de um carro de fórmula 1 do campeonato de 2012, este tem de aguentar um ensaio estático definido pela Fédération Internationale de l'Automobile (FIA), a instituição que governa a competição. Por este motivo, neste trabalho são também acompanhados os procedimentos de teste que se seguem à fabricação do componente.

Este trabalho foi desenvolvido no nível empresarial. Mais especificamente nas instalações da empresa Optimal's Structural Solutions lda. Consequentemente, constrangimentos de tempo e custos podem por vezes adiar estudos mais detalhados que possivelmente se realizariam em ambiente académico. De qualquer forma, todos os estudos necessários foram realizados neste trabalho.

**Palavras-chave:** Optimização topológica, Análise de contacto, modelo não linear de material, OptiStruct, Análise geometricamente não linear.

# Abstract

In this work a topology optimization, with the objective of minimizing weight, is performed to a metallic component that undergoes material plastic deformation. The topology optimization is performed by combining the use of commercial codes with manual optimization.

This component is loaded by circular shape metallic pad. For this reason, a contact analysis between these two parts is modeled. Deformations during loading are considerable and the material linear elastic region is overshoot; thus geometric non-linear analysis with material non-linear behavior are also performed with the use of commercial codes.

Since this piece is an important part of a Formula 1 car of the 2012 championship, it must withstand a statical test defined by the Fédération Internationale de l'Automobile (FIA), the competition governing body. Thus the testing and manufacturing procedure have also been closely followed.

This work was developed in the corporate level. More specifically at Optimal's Structural Solutions lda facilities. As a consequence, time and cost constraints sometimes holds back further and more detailed analysis that would possibly be made in an academic environment. Regardless, all the necessary analysis have been made in this study.



**Keywords:** Topology optimization, Contact analysis, Non-linear material model, OptiStruct, Geometric non-linear analysis.

# Contents


Acknowledgments . . . . . v
Resumo . . . . . vii
Abstract . . . . . ix
List of Tables . . . . . xiii
List of Figures . . . . . xvi
Acronyms . . . . . xvii
Nomenclature . . . . . 1

**1 Introduction** **1**
1.1 Roll Hoop . . . . . 1
1.2 Objectives . . . . . 2
1.3 Literature Review . . . . . 2
1.4 Thesis Structure . . . . . 3

**2 The Optimization Problem** **5**
2.1 The Roll Hoop . . . . . 5
2.1.1 Dimensions . . . . . 6
2.2 The Monocoque . . . . . 6
2.3 Technical Regulations . . . . . 9

**3 Numeric Tools and Optimization** **13**
3.1 Finite Element solver . . . . . 13
3.2 Topology Optimization . . . . . 14
3.3 Non-linear analysis with contact and material plasticity . . . . . 18
3.3.1 Non-linear analysis in Abaqus . . . . . 18
3.3.2 Contact . . . . . 20
3.3.3 Non-linear material model . . . . . 25
3.4 Linear Buckling . . . . . 25

**4 Results** **27**
4.1 Finite Element Models . . . . . 27
4.2 Iteration 1 - Topology Optimization . . . . . 29

4.2.1 Optimization Setup . . . 30
4.2.2 Optimization Results . . . 31
4.3 Iteration 2 - Structural Linear Analysis . . . 33
4.3.1 New Geometry Description . . . 33
4.3.2 Model and Results . . . 35
4.4 Iteration 3 - Structural Linear Analysis . . . 38
4.4.1 New Geometry Description . . . 38
4.4.2 Model and Results . . . 40
4.5 Iteration 6 - Geometric Non-Linear Analysis with Contact Interaction and Material Plastic Behaviour . . . 42
4.5.1 New Geometry Description . . . 42
4.5.2 Model and Results for Linear Analysis . . . 44
4.5.3 Model and Results for Geometric Non-Linear Analysis With Material Plastic Behaviour and Contact Interaction . . . 48

**5 Testing and Results** **53**
5.1 First Attempt . . . 54
5.2 Second Attempt . . . 54
5.3 Third Attempt . . . 55

**6 Conclusion and Further Work** **60**
6.1 Conclusion . . . 60
6.2 Achievements . . . 60
6.3 Further work . . . 61

**Bibliography** **64**

# List of Tables

4.1 Material properties. . . . . 29
4.2 Model information and optimization set up. . . . . 31
4.3 Iteration 2 model characteristics. . . . . 35
4.4 Iteration 3 model characteristics. . . . . 40
4.5 Iteration 6 model characteristics. . . . . 45
4.6 Eigenvalues from buckling analysis. . . . . 48

5.1 Second repair model characteristics. . . . . 58

6.1 Weight evolution along the iterative process. . . . . 60

# List of Figures


1.1 Roll hoops used in road cars. . . . . 1
1.2 Roll hoops used in racing cars. . . . . 2

2.1 Roll hoop initial geometry. . . . . 6
2.2 Roll Hoop dimensions (dimensions in mm) - Side view. . . . . 7
2.3 Roll Hoop dimensions (dimensions in mm) - Front view. . . . . 7
2.4 Roll Hoop dimensions (dimensions in mm) - Leg's base. . . . . 7
2.5 Roll Hoop dimensions (dimensions in mm) - Top view. . . . . 8
2.6 Roll Hoop dimensions (dimensions in mm) - Rear view. . . . . 8
2.7 Unmounted monocoque from a 2007 F1 Renault car. . . . . 8
2.8 Required roll structures positioning. . . . . 9
2.9 Projected area on plane 50mm bellow the top of the roll hoop (dimensions in mm). . . . . 10
2.10 Loading surface. . . . . 10

3.1 Checkerboard examples taken from reference [2]. . . . . 17
3.2 Abaqus methodology for geometric non-linear problems (Newton's method) . . . . . 19
3.3 Node projection in node-to-surface discretization. Picture from Abaqus manual. . . . . 21
3.4 Consequences from correct and incorrect mesh refinements for slave and master surfaces. 21
3.5 Possible contact path with finite sliding. . . . . 23
3.6 Definition of the anchor point for small-sliding used with node-to-surface. . . . . 23
3.7 Incorrect use of small-sliding. . . . . 25
3.8 Material plasticity approximated by portions of linear behaviour. . . . . 26

4.1 3D mesh generation process. . . . . 28
4.2 Roll hoop mesh at loading locations. . . . . 29
4.3 Roll hoop's supporting base. . . . . 29
4.4 Roll hoop in original shape. . . . . 30
4.5 Optimization output. Elements density. . . . . 31
4.6 Optimization results. Elements density. . . . . 32
4.7 Main load path. . . . . 32
4.8 Checkerboard and buckling considerations. . . . . 33
4.9 Iteration 2 geometry. . . . . 34

4.10 Iteration 2 geometry dimensions (dimensions in mm). . . . . 35
4.11 Iteration 2 results for forward and rearward load load cases. . . . . 36
4.12 Von Mises stresses with areas of greater concern highlighted (load cases envelope). . . . 37
4.13 Least stressed areas (load cases envelope). . . . . 37
4.14 Load cases displacements. Deformations amplified 3 times. . . . . 38
4.15 Geometry evolution between iterations 2 and 3 (dimensions in mm). . . . . 39
4.17 Solid reinforcement on load application area. . . . . 39
4.16 Skin and ribs thickness comparison between iteration 2 and 3 (dimensions in mm). . . . . 40
4.18 Von Mises stresses (load cases envelope). . . . . 41
4.19 Load cases displacements. Deformations amplified 3 times. . . . . 42
4.20 Skin and ribs thickness comparison between iteration 3 and 6 (dimensions in mm). . . . . 43
4.21 Geometry evolution between iterations 3 and 6 (dimensions in mm). . . . . 44
4.22 Video camera support and leg-roll hoop fillet details. . . . . 44
4.23 Holes for bolted unions. . . . . 45
4.24 Model used for hoisting load case. . . . . 45
4.25 Von Mises stresses (load cases envelope). . . . . 46
4.26 Von Mises stresses for the bond layer (load cases envelope). . . . . 47
4.27 Von Mises stresses (nose up and nose down envelope). . . . . 47
4.28 Displacement plot for buckling results. . . . . 48
4.29 Model for non-linear analysis. . . . . 49
4.30 Von Mises stresses for geometric non-linear analysis (load cases envelope). . . . . 50
4.31 Unrealistic hight strains due to excessively deformed element. . . . . 51
4.32 Maximum principal plastic strains. Load cases envelope for geometric non-linear analysis. 51
4.33 Von Mises stresses for the bond layer (load cases envelope). . . . . 52

5.1 Static test apparatus. . . . . 53
5.2 Dented roll hoop. . . . . 54
5.3 Cracks formed during testing. . . . . 54
5.4 Iteration 6 and 6.1 FEM comparison. . . . . 55
5.5 Von Mises stress comparison between iteration 6 and 6.1 (load cases envelope). . . . . 56
5.6 Crack created during the second attempt. . . . . 56
5.7 Second repair geometry vs iteration 6 geometry. . . . . 57
5.8 Leading edge section increase with second repair (dimensions in millimeters). . . . . 57
5.9 Von Mises stress for forward load load case. . . . . 58
5.10 Von Mises stress for rearward load load case. . . . . 58

# Acronyms

**CFRP** Carbon Fibre Reinforced Plastic

**CAD** Computer Aided Design

**FE** Finite Element

**FEM** Finite Element Model

**FEA** Finite Element Analysis

**RBE** Rigid Body Element

**SIMP** Solid Isotropic Material with Penalization

# Nomenclature

### Greek symbols

| | |
|---|---|
| $\lambda_n$ | Eigenvalues. |
| $\Omega$ | Design domain. |
| $\rho$ | Element density. |
| $v_n$ | Eigenvectors. |

### Roman symbols

| | |
|---|---|
| $c$ | Displacement correction. |
| $f$ | Objective function. |
| $g$ | Constraints function. |
| $K_G$ | Geometric stiffness matrix in the deformed shape. |
| $U$ | Displacement vector. |
| $V$ | Material volume. |
| $p$ | Penalization factor. |
| $\underline{K}$ | Penalized stiffness matrix. |
| $K$ | Element original stiffness matrix |

### Subscripts

| | |
|---|---|
| $i, j$ | Computational indexes. |

# Chapter 1

# Introduction

In this chapter the reader is presented to a roll hoop, the object of study of this thesis. Afterwards the objectives established for this work are explained, followed by the literature review and thesis outline.

## 1.1 Roll Hoop

The roll hoop is a safety structure, used in the automotive industry. This structure is used in open roof vehicles, like convertibles or cars with no roof, and it is designed to protect the driver and passengers from harm in case the vehicle rolls over.

Roll hoops are generally placed behind the occupants head and may take many shapes and sizes depending on the vehicle characteristics. The following pictures show a few examples of roll hoops used in road and racing cars.

(a) Convertible car

(b) Car with no roof

Figure 1.1: Roll hoops used in road cars.

In Racing cars is frequent to see roll hoops that accumulate both structural and aerodynamic functions like the examples from figure 1.2. This strongly influences the shape of the piece, which many times dictate the material and construction method used in its fabrication.

Rolls hoops play an important safety role and must be capable of withstand severe loading. For this reasons they undergo careful structural studies to assure its function is done properly.


(a) Structural function


(b) Structural and aerodynamic function

Figure 1.2: Roll hoops used in racing cars.

## 1.2 Objectives

The objective of this thesis is to report the topological optimization done to a roll hoop used in a 2012 Formula One car. As a resemblance to the aeronautic industry, Formula One is a very demanding and highly competitive discipline that requires efficient and light weight structures in oder to achieve interesting results. For this reason the optimization here preformed aims to obtain the lightest possible roll hoop that successfully performs its mission.

In order to do so, in this work are performed several different studies to the roll hoop such as: linear static, geometric non-linear with material plasticity, contact and bucking analysis.

This structural optimization and all the associate calculations were performed by the company Optimal Structural Solutions lda, while the design/CAD work was performed outwards of this company. In the end the final product passed the required testing established by the Fédération Internationale de l'Automobile (FIA).

## 1.3 Literature Review

Here is a quick historical revision of the publications that lead to the creation of methods and tools vital to success of this work.

Topology optimization is not new concept once the first paper published on the subject was back in 1904 by Michell [1]. However it was only in the 70's that publications on the issue started to appear more often. Some classic references on the subject are the books of Hemp [12], Rozvanys [13] and [14], published in 1973, 1989 and 1976 respectively. Since then, and together with the development of computing power, the interest on topology optimization grew both for investigators and the industry, and ever since developments on the subject continued to appear along the years. Nowadays there are many theories and methods about it and the work of Bendsøe and Sigmund [2] is a good review of the most relevant.

Presently one of the most popular Finite Element (FE) based methods for topology optimization is the Solid Isotropic Material (or Microstructure) with Penalization (SIMP). The idea behind this powerful

method was first presented by Bendsøe [7] in 1989, and ever since many other articles and books have been published on the subject. Today SIMP is widely used by the majority of commercial Finite Element Analysis (FEA) codes, such has Optistruct (the one used in this work), MSC/Nastran, Ansys, Genesis, Abaqus, etc.

The first works on the concept of finite elements were published by Courant [15] and Hrenikoff [16]. Hrenikoff introduced the concept of the frame work method, where a plane elastic medium was modeled as a set of beams and bars, and Courant, by means of continuous functions defined in a subdomain, defined a triangular assemblage to study the St. Venant torsion problems. However the formal presentation of the method is attributed Turner, Clought, Martin and Topp [17] and Argyris and Kelsey [22] . Later Clough [23] used the term finite elements that lives till today.

## 1.4 Thesis Structure

This work is divided in six chapters with the following contents.

Chapter 2 presents the roll hoop which is, the component that will be the subject of this optimization problem. All the technical considerations that affect and limit the optimization process are also here explained, such as manufacturing constraints, integration of the roll hoop on the car and the FIA technical regulation that all the cars must respect in order to compete in the formula 1 2012 championship.

In chapter 3 we approach the numerical tool used to perform the optimization as well as the relevant theoretical methods embedded in this that were necessary to perform this study.

Chapter 4 reports the most relevant numerical calculations and iterations that characterized the optimization work performed.

In chapter 5 are presented the results from the mandatory static tests that must be performed to the roll hoop in order for this to be certified by FIA. Together with the results, are also described the drawbacks that arise during the manufacturing and testing, and how these were overcome.

To finalize, chapter 6 resumes the overall progress achieved along the course of this work, together with the most relevant results and conclusions learned.

# Chapter 2

# The Optimization Problem

In the this chapter is presented the roll hoop in its initial geometric shape, as well as other relevant components, together with the required certification testing established in FIA's 2012 Formula One Technical Regulations document.

## 2.1 The Roll Hoop

The roll hoop subjected to optimization in this work is the one presented in figure 2.1. This geometry is the starting point of this work and defines the design space for the optimization process. From now on we must assume that all the material is inside the shell of this geometry, and no more material can be added.

As suggested by its circular shape, this particular roll hoop also serves as an air intake for the car engine compartment which is located further back and lower to this component. The combination of these two functions has proven to be an efficient and frequently used solution by many teams for several years.

The roll hoop is glued to the car's monocoque in its two front legs and rear support. However to assure a more robust union the two parts are also bolted one to the other. Anyhow, in this first iteration, the roll hoop does not have the holes for the bolted joint. The placement of these is left for a later stage of the optimization process where we know better the most stressed regions, and the geometry of the roll hoop is further developed.

Some teams make roll hoops of carbon fibre reinforced plastic (CFRP), which is a famous material for having a low density and high strength. However is hard to manufacture complex geometries with it. Because metallic components are easier to manufacture, is possible to create complex geometries that many times out perform the use of lighter materials like CFRP; for this reason this roll hoop is made of metal alloy.

Fortunately the manufacturing process used to fabricate the roll hoop imposes very little barriers to its design, once this piece will be sintered by a 3D printer. This technology allows the fabrication of extremely complex geometries and imposes very little fabrication constraints; a feature that comes very

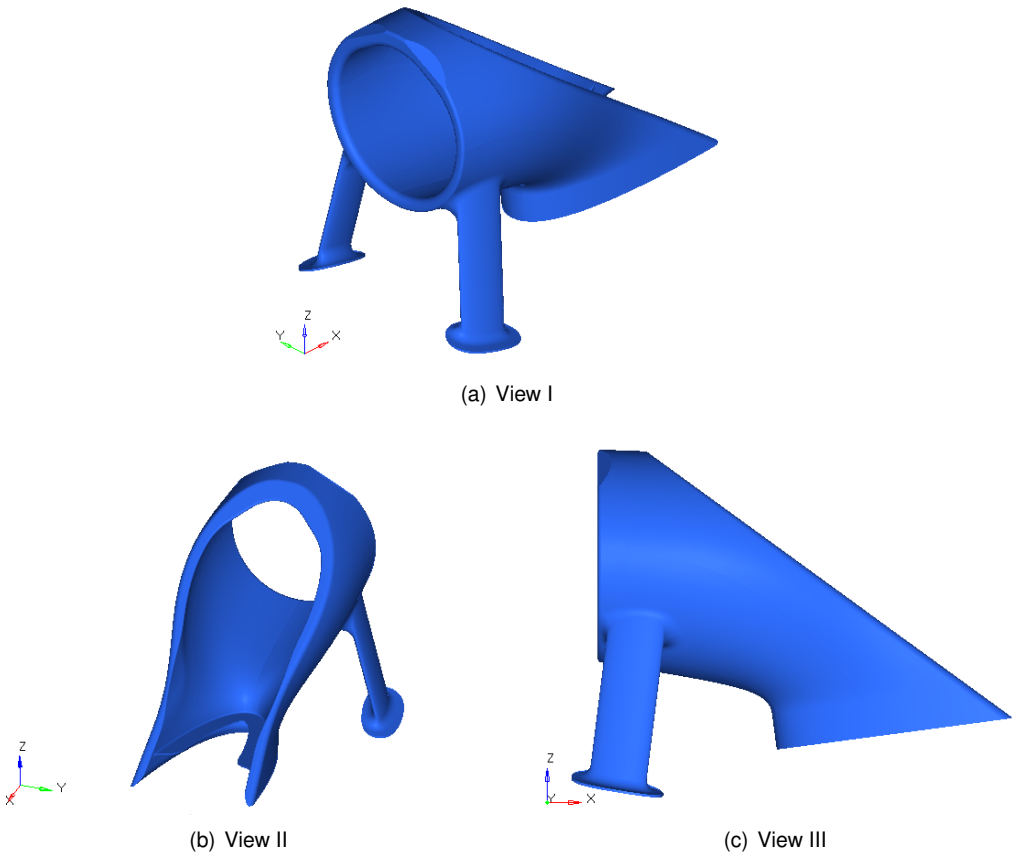


(a) View I

(b) View II

(c) View III

Figure 2.1: Roll hoop initial geometry.

handy when is desired to obtain optimum shapes. Still there are a few considerations to account during the design process but we will get there later on.

### 2.1.1 Dimensions

Here is a short description of the most relevant dimensions for the starting point roll hoop.

## 2.2 The Monocoque

The monocoque is the car's central and main structure and it has two vital functions. The first is to protect the pilot, in a crash situation, once the driving seat is inside the monocoque; secondly it unifies several crucial components of the car such as fuel tank, front wings, front suspension and engine. The engine also plays an important structural role once the rear suspension and wings are bolted to it.

The word monocoque comes from the greek for single *(mono)* and french for shell *(coque)*, and is often used in structures based on the concept of stressed skin. As the name suggests, in such structures the load is supported through the component's skin. The car's survival cell, as well as the majority of nowadays aeronautic structures, makes use of this concept and for this reason the name monocoque was adopted.

This part is made of CFRP and, for the pourpose of this work, we will assume that this component is

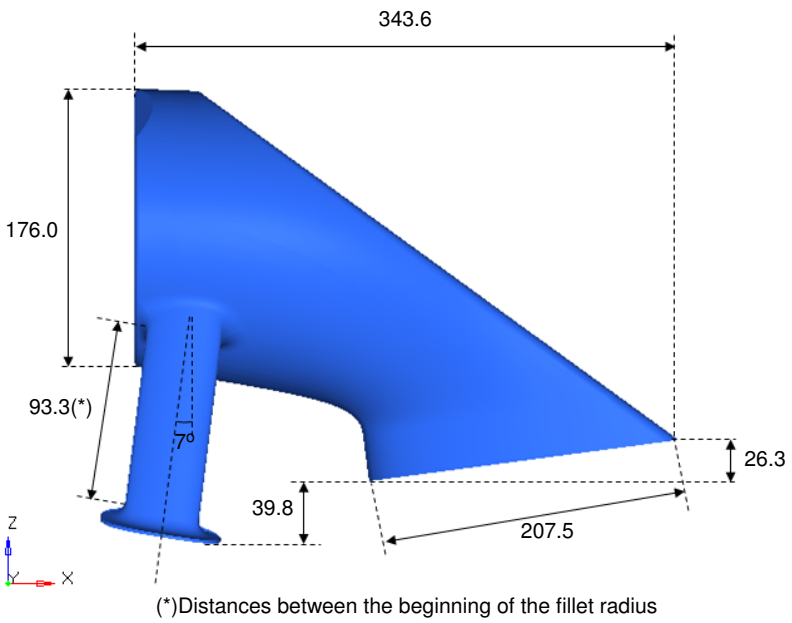


Figure 2.2: Roll Hoop dimensions (dimensions in mm) - Side view.

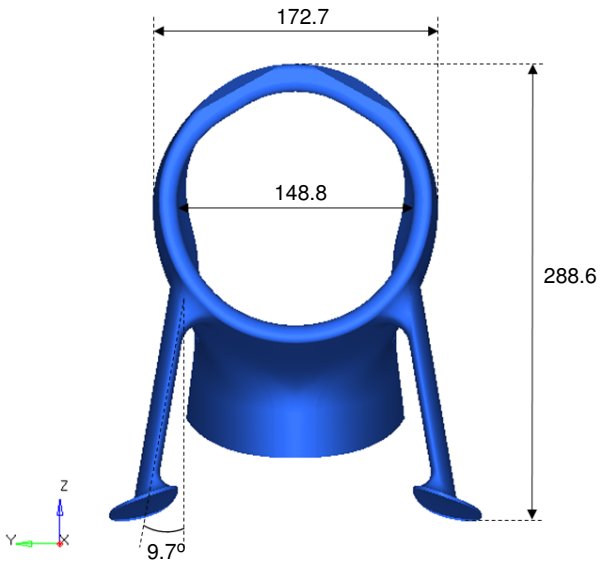


Figure 2.3: Roll Hoop dimensions (dimensions in mm) - Front view.

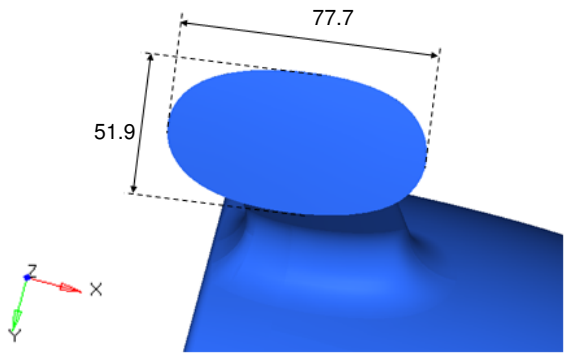


Figure 2.4: Roll Hoop dimensions (dimensions in mm) - Leg's base.

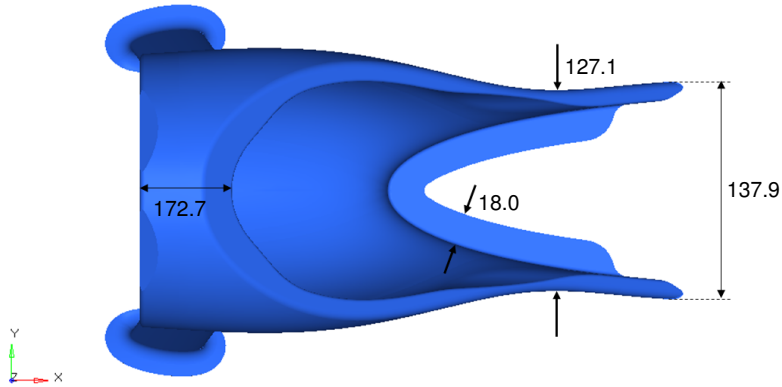


Figure 2.5: Roll Hoop dimensions (dimensions in mm) - Top view.

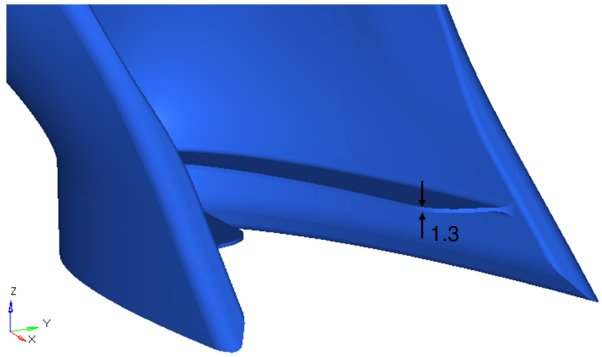


Figure 2.6: Roll Hoop dimensions (dimensions in mm) - Rear view.

strong enough to withstand the loads that will be transmitted by the roll hoop. To have a better perception of the geometry of this vital component, figure 2.7 shows the monocoque of a 2007 F1 Renault car when this is not mounted to the engine (mounted in the back), nose and front suspension.


Figure 2.7: Unmounted monocoque from a 2007 F1 Renault car.

## 2.3 Technical Regulations

Formula One is a sport regulated by the FIA which, previously to the beginning of the season, publishes the technical regulations that govern the competition during the upcoming year. Any given car competing in the event must obey these regulations and pass all the required testing established in the same.

Several rules and strength tests are established specifically for roll hoop structures. This constraints strongly influence the roll hoop's final result. For this reason, all the relevant norms are here explained.

### Geometry and positioning

A formula one car must have a primary and secondary roll structures. Both pass in the car centerline and the secondary is placed in front of the primary (see figure 2.8). For the purpose of this work only the primary (the so called roll hoop) is studied but for the sake of clearness the two are here referenced.

According to chapter 15.2 of reference [5], the principal structure must be at least 940mm above the reference plane at a point 30mm behind the cockpit entry template. The reference plane is defined by the monocoque's lowest point. The second structure must be in front of the steering wheel but no more than 250mm forward of the top of the steering wheel rim in any position.

The two roll structures must be of sufficient height to ensure the driver's helmet and his steering wheel are at least 70mm and 50mm respectively below a line drawn between their highest points at all times has represented in figure 2.8.

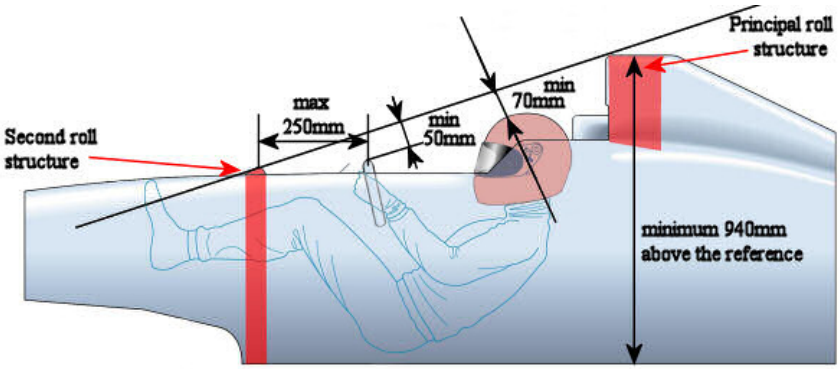


Figure 2.8: Required roll structures positioning.

The principal roll structure must have a minimum enclosed structural cross section of 10000mm$^2$, in vertical projection, across a horizontal plane 50mm below its highest point. The projected area must not exceed 200mm in length or width and may not be less than 10000mm$^2$ below this point. According to measurements from finite element data the roll hoop respects this geometric constraints as shown in figure 2.9.

### Loads

The roll hoop must undergo a static test where a combined load of 119,16KN is applied in the top of the roll hoop's structure by a rigid and circular flat pad. The pad has has a diameter of 200mm

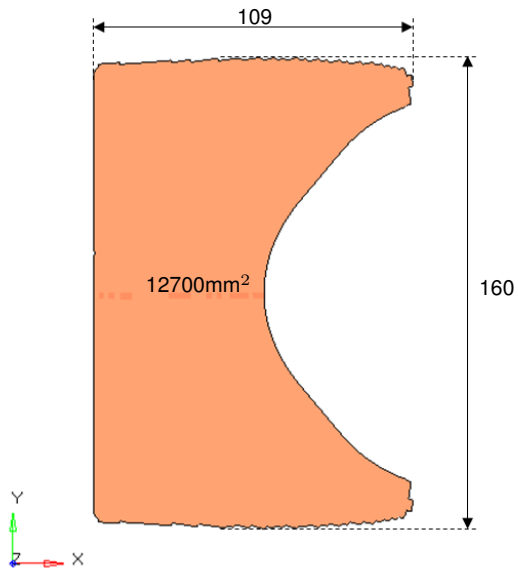


Figure 2.9: Projected area on plane 50mm bellow the top of the roll hoop (dimensions in mm).

and it's surface is perpendicular to the loading direction. This load is the combination of 50KN in the lateral direction (perpendicular to the car's traveling direction), 60KN longitudinally (opposite to the car's traveling direction) and 90KN vertically in downwards direction. To better accommodate such force the roll hoop as two loading surfaces parallel to the loading pad as shown in figure 2.10.

For the test to be valid, peak load must be applied in less than 3 minutes and maintained for 10 seconds. Deformation under loading must be less than 25mm measured along the loading direction, and structural failure is limited to 100mm bellow the top of the structure measured vertically. The roll hoop must be attached to the survival cell (monocoque) while this is supported in its underside, by a flat plate, and laterally by specially made load test pads. To protect it's surface 3 mm rubber can be used between the loading pad and roll hoop.

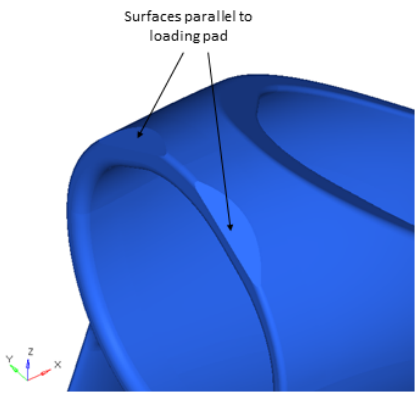


Figure 2.10: Loading surface.

Is also mandatory to present detailed calculation demonstrating that the roll hoop also withstands the same load when the longitudinal component is applied forwards (60KN applied in the car's traveling direction).

Is frequently necessary to use a crane to hoist the car whenever this is not capable to move on its

own. For these situations the hoisting point used is precisely the roll hoop and thus is also necessary to assure that this component is though enough to withstand such load.

The FIA does not provide any loads cases to study this situation, leaving the teams the responsibility of doing it. In our case we consider the situation where a fully loaded car, (driver and full fuel tank) with an approximate weight of 820Kg, suffers a 3G acceleration (29.4$m/s^2$) in the upwards direction. From this results a 24.1 KN load that is applied in the underneath of the roll hoop. In Chapter 4 a more detailed explanation of this load cases is provided.

# Chapter 3

# Numeric Tools and Optimization

Nowadays the finite element method plays a crucial role in several engineering disciplines and structural analysis is no exception. For this reason we present in this chapter the finite element strategies used in this work. The reader is also presented an introduction to basic optimization concepts and topology optimization.

## 3.1 Finite Element solver

### RADIOSS [3]

RADIOSS is the finite element solver used in this work for the majority of iterations. This solver is both capable of solving linear and non-linear simulations and it can be used to simulate structures, fluid, fluid-structure interaction, sheet metal stamping and mechanical problems.

From the user point of view, RADIOSS is very similar to the popular solver Nastran. This is not only because RADIOSS is compatible with Nastran input data, but also because both use essentially the same sparse matrix and Lanczos methods. As a consequence, both solvers take similar computation time and present similar results.

RADIOSS comes integrated in the software package HyperWorks which, on its turn, contains several other softwares used along the different engineering stages. Some of the most relevant for this work are a mesh generator and pre-processor by the name of Hypermesh, a post-processor called Hyperview and the structural optimizer named OptiStruct. The release version used in this work is the HyperWorks 10.

The use of RADIOSS is not a new event in the history of Optimal's existence. This software has been used in other projects with good final results and fulfilling the demanded requirements. Besides, its similarities with Nastran (probably the most popular FE solver for linear analysis in the aeronautic industry) go from the user point of view to the final result, giving us the confidence in this solver to perform the majority of calculations for this work.

### Abaqus [4]

Although capable of performing geometric non linear analysis, RADIOSS and Nastran do not have such a good performance in this kind of studies [18]. For this reason the FE solver used for geometric non linear analysis is Abaqus. This solver is famous for its capabilities on the non-linear domain, not only because of its accuracy but also due to the reliable algorithms that automatically help stabilizing the calculus process.

Also providing a considerable asset is a previous good experience with the software and the already existing know-how to perform this analysis with Abaqus.

## 3.2 Topology Optimization

In topology optimization we are interested in obtaining the optimum material layout to perform a certain structural function. There could be several reasons to do so such as reduce the components weight, improve the component compliance, use the minimum material possible etc.

Nowadays there are various and very powerful commercial codes to perform structural optimization. However in order to properly exploit their potentials is essential to know some basic concepts of numerical optimization. For this reason a brief explanation of some of these is presented in the following.

A structural optimization problem is controlled by several parameters used to evaluate, control and guide the optimization process. These parameters are an objective function, a design space, design variables and constraints.

The objective function is the cost function and the parameter that we want to optimize either by maximizing or minimizing its value. As its name says the objective function is the goal or the main focus of the optimizer. In our case, for example, the objective is to minimize the roll hoop's weight, thus our objective function will have a numeric value (cost) associated to its weight and the optimizer will try to reduce the value of this parameter to a minimum.

The design domain is the region where optimization will be performed. In our situation the design domain is the majority of the volume defined in figure 2.1.

The design variables are the set of variables that actually implement the changes in the design domain. Continuing with the example of the previous paragraphs, the design variables could be defined in such a way that the legs were now made hollow. However in a different situation from the one of the previous example, a design variables could be defined in other way such that it would have a different effect on the design domain besides a geometric change. As an example in [8] and [9] design variables values not only influenced the geometry's topology as, together with other parameters, could dictate the removal or reintroduction of elements from the mesh.

Several different constraints can be defined for a structural optimization problem. As an example we can impose maximum/minimum displacement of a given FE node/s, or demand a minimum structural compliance or maximum stress in elements. The baseline is that constraints help establishing limits in the optimization process preventing it from going into undesired regions.

Only the correct definition of all this parameters can make the use of commercial codes fruitful. However when one is capable of doing so, the results are often rewarding and spare the user from many hours of iterative process that otherwise would have to be done manually. Nonetheless no optimizer can assure that a given solution is the best solution possible, once the majority of optimization problems are highly multimodal and composed of multiple variables that are practically impossible to fully explore.

## OptiStruct [3]

OptiStruct is the structural design optimizer used in this work and, as said before, comes with HyperWorks 10. Is important to notice that OptiStruct is not a FE solver. Instead, it uses the analytical capabilities of RADIOSS and MotionSolve[1] to compute responses for optimization. As a consequence, the iterative optimization process is a continuous alternation between RADIOSS and OptiStruct. Results computed from RADIOSS are processed by OptiStruct, where objective and constraints are evaluated, and new design variables are defined. With this new variables a new solution to the problem is computed by RADIOSS and the process is repeated until an optimum solution is found.

OptiStruct is capable of performing Topology, Topography, Size and Shape optimization. However, since we are only interested in topology optimization, we will only focus on the features associated with this type of optimization.

In structural topology optimization problems, it might be necessary to add or remove material from the design domain in order to perform the optimization. There are several methodologies to simulate/reproduce this material removal or addition in the finite element mesh. Nonetheless we are going to focus our attention on the Solid Isotropic Material with Penalization method once it is the one implemented in OptiStruct.

### Solid Isotropic Material with Penalization (SIMP)

The SIMP method was first introduced in 1992 by Rozvany [10] although, according to this author in [6], the basic idea behind the method was first proposed by bendsøe [7] in 1989. Nowadays SIMP is one of the most popular and effective methods used in structural optimizers once it simulates the material removal and reintroduction from a finite element mesh. In this method a continuous variable, called density ($\rho$), is attributed to each element in the mesh. This variable is within the range [0,1], and associated to it is the stiffness matrix of a given element as described by the equation

$$\underline{K}(\rho) = \rho^p K, \qquad p > 1, \tag{3.1}$$

in which $K$ and $\underline{K}$ represent the element original stiffness matrix and penalized stiffness matrix, respectively, and $p$ is a penalization factor, which we explain in the following.

Typically, topology optimization problems involve volume constraints. Attributing to our design domain the variable $\Omega$, in any given iteration step we want to determine the volume $V$ of material in $\Omega$. The

[1] Like RADIOSS MotionSolve is a numeric solver that comes with HyperWorks 10. MotionSolve is used to solve multi-body dynamics of mechanical systems.

density parameter is then used to compute this value with the equation

$$\int_{\Omega} \rho(x) d\Omega \leq V, \qquad 0 \leq \rho(x) \leq 1, \qquad x \in \Omega. \tag{3.2}$$

Thus $\rho$ is named density because it is used to compute the structure's volume.

It is important to notice that since $\rho$ is a continuous variable ranging from 0 to 1, we can have intermediate densities that will result in intermediate stiffnesses which are not easily manufacturable. For this reason is important to mitigate intermediate densities in order to approximate the optimal structure to a discrete 0-1 solution. This is done by setting the variable $p \geq 1$; consequently an intermediate density element will have a considerably low stiffness when compared to its cost (volume) making it unfavorable from the optimizer point of view. As a consequence intermediate density elements are automatically penalized without using any explicit penalization schemes. For problems where volume (or any other variable that depends on the volume) is an active constraint is possible to achieve results near the 0-1 solution. In order to do so is usually required $p \geq 3$ [2].

In the SIMP method, $\rho$ is the design variable, and there will be as much design variables as number of elements in the design domain.

#### Disadvantages and issues of the SIMP method

In the following we briefly explain some of the most relevant disadvantages and drawbacks of SIMP.

Because SIMP requires a design variable for each element in the design domain computational problems associated with lack of memory may be a problem, specially in problems with a large number of elements. Besides, a high number of design variables makes harder to reach a global optimum solution because many local minima may be present. This problem takes even greater dimension considering the continuous increase in complexity and size of modern FE models.

Other typical drawback often seen when using SIMP is checkerboard design. This phenomena is recognizable when several layers of elements are alternately distributed between voids and fully dense elements creating a checkerboard like appearance as seen in examples from figure 3.1. This design results from the artificial stiffness and strength of checkerboards that a finite element mesh missmodels. If we consider the stiffness of a plate, of a certain area, that is completely filled with material, the same plate with a checkerboard layout would be half as stiff, or from other perspective, it would have the stiffness of the same fully filled mesh but with half the thickness. With this said, when in the presence of checkerboards one should count for a considerable reinforcement of material in the given area.

Mesh dependence is another issue of the SIMP method. In this strategy the optimizer inputs and outputs come directly from and onto the element mesh. This means that the same problem solved with different meshes might result in different solutions. In other words, if the mesh is to coarse the problem physics might not be properly modeled or the optimizer might not have a fine enough element resolution to draw the best design.

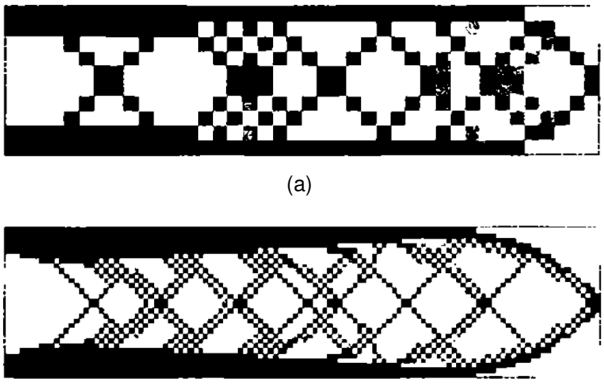

(a)

(b)

Figure 3.1: Checkerboard examples taken from reference [2].

**Implementation in OptiStruct**

In OptiStruct the optimization problem is implemented in the form bellow,

$$\begin{cases} minimize & f(\rho) = f(\rho_1, \rho_2, ..., \rho_n) \\ g_j(\rho) \leq 0, & j = 1, ...m \\ 0 \leq \rho_i \leq 1, & i = 1, ..., n \end{cases} \tag{3.3}$$

in which $f$ is the objective function, $g_j$ is the constraint function and $\rho$ is the design variables vector.

Processing all the constraints and design variables can be a time consuming and computationally expensive, specially in the cases of gradient-based topological optimizations with large numbers of design variables and constraints. To make this task easier to manage OptiStruct uses a method named constraint screening [3] that trims down the number of optimization responses to a representative set. In this process, responses that are far from their limit bound (non active constraints) or less critical than others of the same type, same design region and subcase are considered not to affect the direction of the optimization. For this reason these responses are ignored in the current design iteration, saving a considerable amount of time.

For this process to work it requires a good trade-off between ignored responses and time saving: considering only a few responses may take more iterations to converge, while the opposite may be too time consuming. By default OptiStruct considers only the 20 most critical constraints that come within 50% of their bound for each response type, each region and each subcase.

As the optimization iterations build up, a convergence evaluation algorithm is necessary to asses the converging status of the process. To do so, OptiStruct performs two convergence tests named regular convergence and soft convergence [3]. If any of this tests is satisfied OptiStruct assumes that the solution has converged.

Regular convergence is considered when variation changes in the objective function are less than the objective tolerance and constraint violations are less than 1% for two consecutive times. Taking in consideration that to compute one variation change of objective and constraints we need two consecutive iterations, it is required to have at least three consecutive iterations to calculate two variation changes.

The design is considered unfeasible when, for three consecutive iterations, constraints remain violated by more than 1% with a violation change less than %0.2 and the change in the objective function is less then the objective tolerance.

Soft convergence is achieved when, for two consecutive iterations, little or no change is verified in the design variables.

## 3.3 Non-linear analysis with contact and material plasticity

From the static test described in section 2.3, it is known that the roll hoop deforms considerably and that the stresses get dangerously close to the material's yield and ultimate strength. Besides, it is also important not to forget the effect of the contact between the loading pad and the roll hoop. For those reasons a geometric non linear analysis with material plasticity and contact interference is performed. This analysis is also the most reliable calculation to asses if the maximum allowed displacement of 25mm is not violated, because not only accounts for the stiffness change that affects a structure during large deformations as it considers the non linear material behaviour at the same time.

### 3.3.1 Non-linear analysis in Abaqus

In the majority of structural problems, the structures do not deform much under loading. In fact this deformation is so small that, for relatively small components, it is not even visible to the naked eye. Thus, the geometric shape of the structure is essentially the same and that means that the structure's stiffness does not change considerably during loading. As a result the load-displacement graphic is a straight line and the structure's behaviour is said to be linear. Also as long as the linear behaviour is verified, and once we know the deflection for a given load, the deflection for a different load can be interpolated from the previous solution.

However, when the geometric deflection or the material behaviour are such that the stiffness of the structure changes the load-displacement graphic is no longer linear but a curve. For non-linear problems the strategy used by the majority of commercial finite element solvers such as Ansys, Abaqus, Nastran, RADIOSS, etc, is to apply the load incrementally and update the geometric stiffness of the structure along the process. This way we are approaching a non-linear behaviour with consecutive linear responses.

In Abaqus this process is made by the use of Newton's method. In each load increment Abaqus attempts to find the structural equilibrium state, by matching the external load/s with the structure's internal force/s (or reaction force/s) for the new deformed shape. Only if those two match or are very close to each other, can we finally say that the structure is in equilibrium. To better understand this process let us consider the example in figure 3.2. Consider that we are loading a given structure with a load $P$; since we expect a geometric non-linear behaviour we a perform non-linear analysis in Abaqus. Thus the load $P$ is divided in 3 or 4 increments that are consecutively applied. Consider that the first and lowest load $P_{inc1}$ is applied and, as shown in figure 3.2, the structure is already behaving non-linearly.

In this case Abaqus will iteratively try to find the equilibrium point between the applied load $P_{inc1}$ and the structure's internal force $I$[2]. To account for geometric non-linear effects the internal forces $I_{it1}$ are calculated with the updated stiffness matrix that outcomes from the new deformed shape associated to displacement $U_1$. The difference $P_{inc1} - I_{it1}$ is the residual $R_{it1}$ for iteration 1, and this is the parameter that will control the iterative process and dictate if the solution has already converged for a given load or not. The lower are the residuals, the closest we are to the true solution.

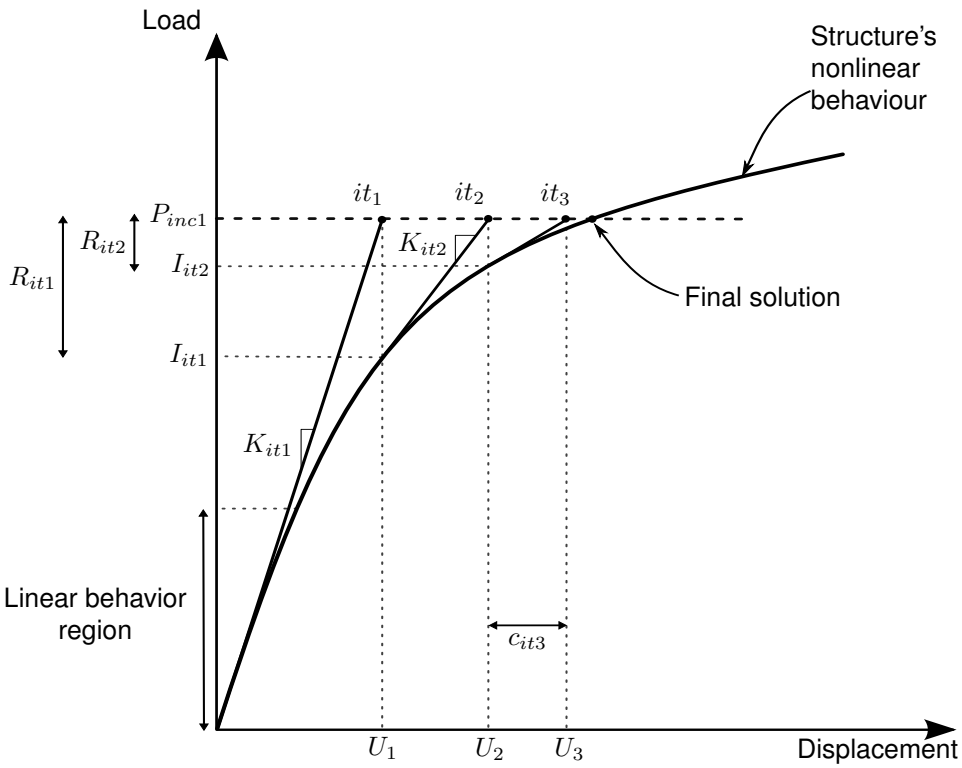


Figure 3.2: Abaqus methodology for geometric non-linear problems (Newton's method)

In order to obtain a good quality solution it is necessary to establish a minimum residual threshold. If this threshold is not respected another iteration is performed as an attempt to bring the residuals down to the acceptable limit. This is the case of iteration 1 (point $it_1$in figure 3.2) where the residual $P_{inc1} - I_{it1}$ is not small enough. In these situations, a new stiffness matrix is computed from the deformed shape given by $U_1$, and the residual forces $P_{inc} - I_{it1}$ are applied in the model. Inverting the new stiffness matrix for the load $P_{inc} - I_{it1}$ results in iteration $it_2$, from which displacement $U_2$ and internal force $I_{it2}$ are obtained, and the residual $R_{it2} = P_{inc1} - I_{it2}$ is computed. If the minimum value for the residual is not respected the whole process is repeated until this is small enough. When the residual from the latest iteration is bellow the established threshold the solution is said to have converged.

[2]Internal force is the conjugation of forces acting on node as a result from the stressed elements attached to it. In order for the structure to be in equilibrium the sum of this forces must be zero. For the particular node/s where external force/s (load/s) are applied, the internal force/s must be equal and of opposite sign to these (reaction force). Here, when we say "structure's internal force", we are referring to this reaction force.

#### Convergence

By default Abaqus considers that the solution has converged when residual forces at any degree of freedom are 0.5% of the applied force, although this value can be changed according to the user's desire.

Besides the residuals, Abaqus has another convergence criteria based on the structure's displacement. For a given iteration $i$, a parameter called the displacement correction ($c_i$) is computed according to equation

$$c_i = U_i - U_{i-1}. \tag{3.4}$$

The displacement correction is then compared to the total incremental displacement given by

$$\Delta U_i = U_i - U_1, \tag{3.5}$$

and for this criteria to be verified $c_i$ must be less than 1% of $\Delta U_i$.

Convergence is only achieved if both residual and displacement criteria are verified.

Depending on the level of non-linearity, the problem might take more or less time/iterations to converge. By default, if solution fails to converge after 16 iterations Abaqus reduces the load increment ($P_{inci}$) to 25% of the previous and attempts to find a converged solution again. If convergence is still not verified the load increment is reduced again by another 25%. The process is repeated until convergence is found. If after 5 attempts convergence is still not found or is the load increment is smaller than the minimum established by the user, Abaqus stops the analysis. If this situation occur it is probably because the problem diverges and such load is not possible to apply to the structure.

### 3.3.2 Contact

Abaqus provides the user with several contact formulations based on a choice of a contact discretization and a tracking approach. The correct choice depends on the type of contact we are dealing with and on the computational cost. Independently of the user's choice, a set of master and slave nodes/surfaces must be defined in order to identify the elements that will be in contact.

#### Contact discretization

To simulate contact between two surfaces, Abaqus applies a series of constraints at several locations on the contact surfaces. The location and how these constraints are defined depends on the contact discretization method used. Abaqus offers two possible contact discretization methods: node-to-surface and surface-to-surface.

#### Node-to-surface discretization

In node-to-surface discretization the nodes from the slave surface interact with their corresponding projection on the master surface. Thus for a given slave node its projection is computed with the nearby

master nodes, such that the resulting projection is always normal to the master surface (see figure 3.3). The slave nodes are then constrained not to penetrate the master surface, although the opposite may occur as exemplified in figure 3.4. From this picture we can also see that is important to have a slave surface at least as refined as the master to avoid penetration of master nodes into slave surfaces.

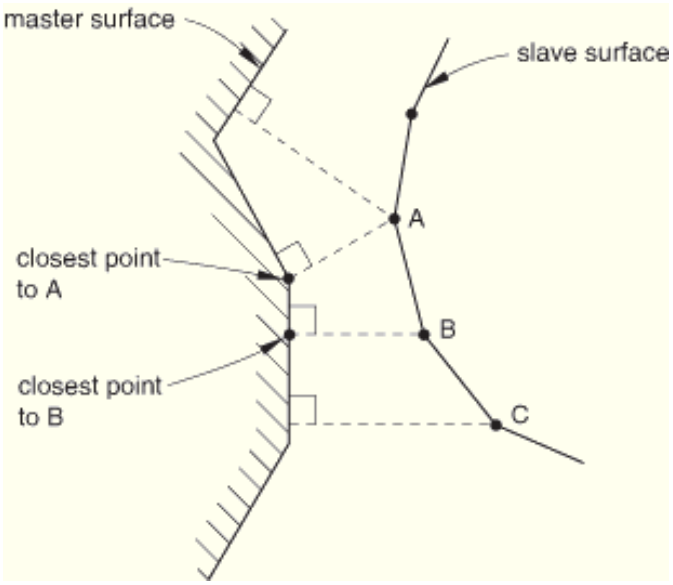


Figure 3.3: Node projection in node-to-surface discretization. Picture from Abaqus manual.

Also, notice that the slave surface normal is irrelevant once contact direction is established according to the master surface normal. For this reason the slave surface can be defined by a set of nodes and the required information for each slave node are its location and the associated area on the master surface.

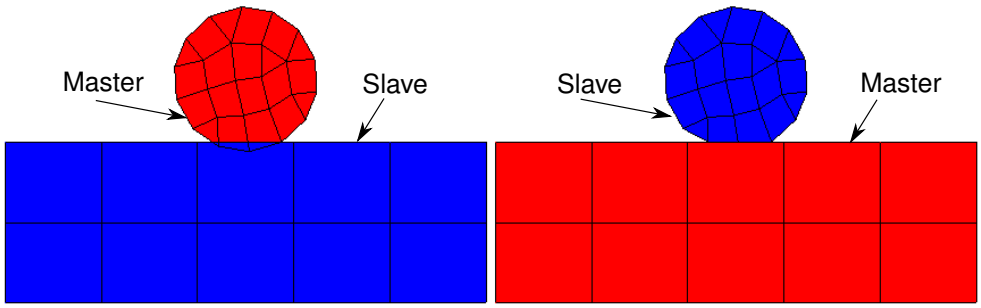


Figure 3.4: Consequences from correct and incorrect mesh refinements for slave and master surfaces.

#### Surface-to-surface discretization

In surface-to-surface discretization the shape of both master and slave surfaces are considered to model the contact interference, since contact direction is based on an average normal of the slave surface region surrounding the slave node. Thus, with this method, contact forces are distributed in an average region of slave surface, and not individual nodes as in node-to-surface discretization.

Independently from belonging to the master or slave surface, with this formulation is possible for some individual nodes to penetrate the other surface. However these penetrations are small and neglectable.

Larger penetrations do not happen without being detected.

#### Node-to-surface vs surface-to-surface

Surface-to-surface discretization usually provides a smoother and more accurate stress distribution than node-to-surface, since contact forces are not concentrated at individual nodes as in node-to-surface discretization. Because contact forces are distributed in an average region of slave surface, surface-to-surface interaction is also less sensitive to mesh refinements and attenuates the differences between slave and master surfaces.

However, surface-to-surface discretization requires more constraints per node, which can increase the solution cost specially in models with large contact areas, or several contact surfaces that interact between each other (a surface that simultaneously acts as salve and master for different pairs of surfaces) or if a master surface is more refined than a slave one. Nevertheless, if this is not the case, the increase in computational cost is not significant.

The differences between both discretization models tend to be attenuated with successive mesh refinements. On the other hand one could argue that because node-to-surface discretization tends to concentrate the load on individual nodes leading to higher peak stresses, this discretization is more conservative which often is a desired characteristic in engineering applications.

#### Contact tracking approaches

Abaqus provides two formulations to model the relative motion between the slave and master surfaces. These are finite-sliding and small-sliding tracking approach and a description of both is presented in the following.

#### Finite-sliding

Finite sliding allows for separation, sliding and rotation of the interacting surfaces as the relative motion goes on. This means that, if a node-to-surface with finite-sliding contact formulation is chosen for a given contact analysis, a possible surface interaction could be the one shown in figure 3.5. As the dashed line represents the trajectory described by the node $N_{s1}$, at time interval t1 the load transfer would be between this node and the element $E_{m1}$. At time step t2 the loaded element would now be $E_{m2}$, and at t4 $E_{m4}$ would be at t3, the node $N_{s1}$ interacted with no other element from the master surface and the load transfer between the two surfaces was null in this node and time step.

For the particular case when finite-sliding is used together with node-to-surface discretization, it is necessary for the master surface to have continuous surface normals at all points, or otherwise, slave nodes may get stuck at the points with this normal discontinuities, leading to convergence problems. To prevent this from happening, Abaqus automatically smooths the surface normals at the required locations. Although this process occurs automatically it is possible for the user to control the level of smoothing applied by Abaqus. If surface-to-surface discretization is used this problem does not happen and smoothing in not required.

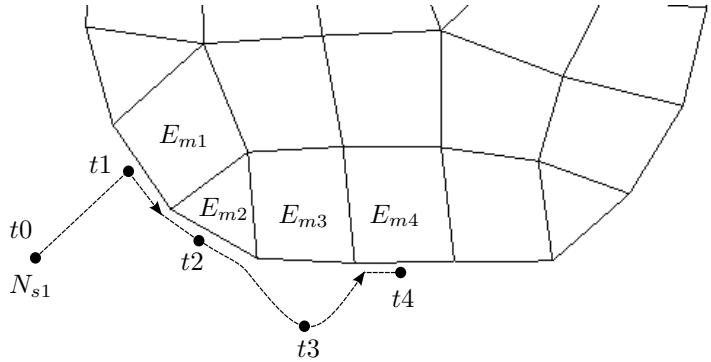


Figure 3.5: Possible contact path with finite sliding.

**Small-sliding**

Small-sliding is the contact tracking approach better suited for problems where the motion between the slave and master surface is small or even null. However, this does not invalidate large deformation and rotation (geometric non-linear behaviour) as long as sliding between slave and master surface is kept small.

Based on this notion, in small-sliding, a given slave node will always interact with the same subset of nearest master nodes throughout the entire analysis. The process where this is defined begins before starting the analysis, while still in the undeformed shape, and for node-to-surface interaction it is defined as follows.

Consider the slave and master surface from figure 3.6. Unit vectors $N_2$, $N_3$ and $N_4$ in the master surface nodes are computed by the average of the unitary normal vectors from adjacent elements. Using the same process, vectors $N_2$ and $N_3$ are now used to compute soothingly variable unitary vectors along the length of element $E_{m2}$. When, at a given point $x_1$, the vector $N(x_1)$ matches the direction of the slave node $1$, the anchor point $x_1$ for this slave node is defined. The anchor point of a given slave node defines the location in the master surface where the interaction between these two will first occur.

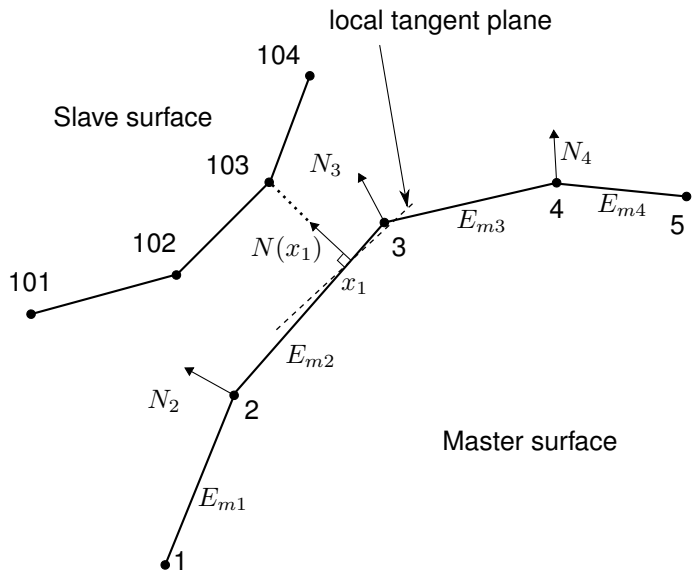


Figure 3.6: Definition of the anchor point for small-sliding used with node-to-surface.

Because Abaqus attempts to associate a planar approximation of the master surface to each slave node, a local contact plane normal to the vector $N(x_1)$ is defined for the node $103$. From this point on, all the contact interaction between salve node $103$ and the master surface, such as load transfer and sliding, happens on this plane. The local contact plane remains fixed relatively to the master surface, but for non-linear geometric analysis its position is updated in order to follow the rotation and deformation of the master surface.

If surface-to-surface discretization is used anchor points are defined as follows: the region around a slave node is projected along the slave surface normal direction onto the master surface. The anchor point is then defined as the center of the area created by this projection. Using node-to-surface or surface-to-surface discretization does not interfere significantly on anchor points location, unless surfaces are considerably distant and non-parallel. If this happens to be the case then small-sliding may not be the appropriate tracking strategy to use.

Once the anchor point is defined, the load from a given slave node will be only transmitted to the nodes that define the plane of the master surface where the anchor was projected to. The load distribution between these nodes is then based on their distance to the anchor point when the slave node contacts the local tangent plane. Going back to the example of figure 3.6, the load from node $103$ will be supported by nodes $2$ and $3$, where more than half is going to node $3$ since this node is closer to the anchor point.

If the anchor point matches the location of a master node, then the load will be shared between these nodes and all the others that share an adjacent facet or element.

As deformation takes place and the slave node slides along the local tangent plane, the load distribution is updated according to the new distances between anchor points and master nodes. However the load will be always transmitted exactly to the same set of nodes, even if the slave node location is not inside the bounds defined by the initial set. This phenomena is visible in figure 3.7 where at time-step $t2$ the slave node is clearly not in contact with initial nodes $2$ and $3$, but the load is still supported by these. This example clarifies how badly small-sliding can model contact when used incorrectly. For this reason it is important to assure that sliding between the master and slave surfaces really is small.

#### Choosing between finite-sliding and small-sliding

As usual this decision depends on the particularities of the problem, since the two approaches were created for different contact situations. Typically small-sliding is an appropriate tracking method if the following conditions are verified:

- Relative sliding between the master and slave surface is within half of the element length, for relatively plane master surfaces, and a fraction of the elements length for highly curved master surfaces.
- Local tangent planes are a good approximation of the master surface geometry even when it is deformed.
- Slave and master surfaces are relatively parallel to each other.

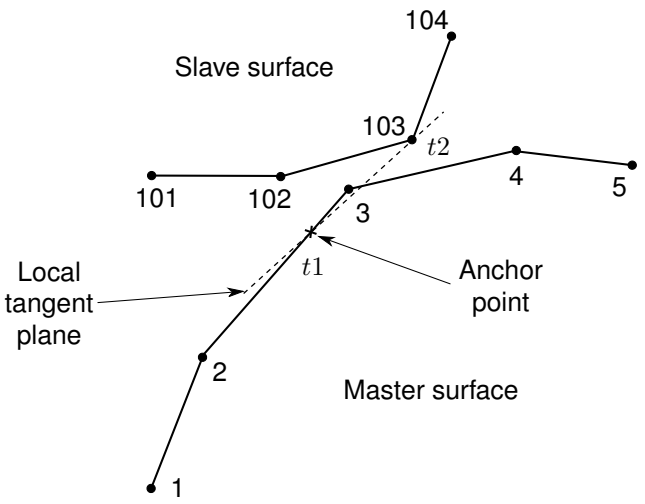


Figure 3.7: Incorrect use of small-sliding.

After the local tangent planes for every slave node is defined, is not required to track for possible contact in other regions of the master surface. For this reason, small-sliding is usually computationally cheaper than finite-sliding, specially for three dimensional problems.

If none of the described conditions is verified then the more general finite-sliding is the best approach to model the contact interaction.

### 3.3.3 Non-linear material model

Abaqus provides several different formulations to model material plastic behaviour. These formulations are compatible for both isotropic and anisotropic materials and include effects of rate-dependent strains and temperature dependence.

In our case we are dealing with an isotropic material which will be slowly loaded at a low temperature. This means that we can reduce our focus to temperature and strain-rate independent material models. Under these conditions, an appropriate material model would be one for which the material elastic modulus is defined linear in strain intervals, as shown in figure 3.8. The yield criteria used for this case is the Mises yield surface [4], [11] and [3]. In brief words, this means that the yield is considered when von Mises stresses are equal or greater than the yield stress[3].

## 3.4 Linear Buckling

Linear buckling analysis was performed the roll hoop to evaluate the possible occurrence of this structural instability during the static test. This calculation was performed with the RADIOSS solver.

To perform this calculation the eigenvalue problem

$$[K - \lambda_n K_G]v_n = 0 \tag{3.6}$$

[3]For more information on the subject please consult section 4.2 from theory reference book of ANSYS 12.0 manual [11]

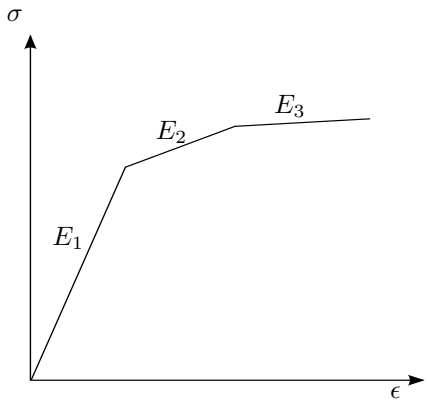


Figure 3.8: Material plasticity approximated by portions of linear behaviour.

is solved. In the above expression $K$ is the geometric stiffness matrix the undeformed shape and $K_G$ is the geometric stiffness matrix after loading/deformation. $\lambda_n$ are the eigenvalues, which can be seen as critical load scale factors or reserve factor (reserve factor is usually defined as the ratio of the allowable load to present load), and $v_n$ are the eigenvectors. Given the eigenvectors, it is possible to plot the representative deformation of the structure during bucking, although not a possible real magnitude of the displacements.

The Lanczos method (for example see [24] and [25]) is used to solve this problem. Other methods, such as the subspace iteration method, are usually faster for few eigenvalues (up to 20 eigenvalues approximately) but both are suitable in our particular case.

Extra care should be taken for cases with closely separated eigenvalues since it usually causes numerical problems [4]. To avoid this inconvenient it is usually helpful to preload the structure (applied a thermal load before applying the mechanical for example). To better understand why this happens lets consider the situation where we apply the preload $P$ given by

$$P = cF, \tag{3.7}$$

being $c$ a scalar constant and $F$ the original structure's load. If the problem is linear elastic the structural stiffness changes to

$$K + cK_G \tag{3.8}$$

and the buckling loads are given by

$$(c + \lambda_n)F. \tag{3.9}$$

This way numerical problems might be eliminated or mitigated.

# Chapter 4

# Results

In this chapter are presented the several results that out come from the iterative optimization performed to the roll hoop. We remind the reader that, although the main focus of this work is the structural calculus and optimization, the final result is a compromise between structural considerations, the component's functionality, manufacturing constraints and design inputs. Thus the end product is not always the best from the structural point of view, but the best blend between all of these considerations.

## 4.1 Finite Element Models

For every iteration described in the following subsections, the same philosophy was used to construct the FE models. For this reason we here describe, with more detail, the methods used to build all the FE models, sparring the reader from repeated information.

Once the roll hoop is considerably thick is would not be appropriate to model it with shell elements. For this reason solid CTETRA elements are used (tetra elements are triangular pyramids and thus have 4 vertices's). The CTETRA elements are automatically created by HyperMesh from a closed volume of shell elements (see figure 4.1). Unfortunately when this method is used is only possible to create CTETRA elements instead of a more efficient [20] [21] CHEXA elements (eight vertices's elements similar to a cube). Considering the complexity of the roll hoops geometry this is the only viable method in order to create the required 3D mesh.

In order to overcome this drawback and to have a more precise model that properly adapts to this geometry, the element size used is 2mm which is a relatively small value. Although it has a heavier computational cost, this small element length allows having more than 1 element through the thickness even in the thinner sections of the roll hoop. Is also advantageous for the optimization process to have a well detailed mesh once it allows the optimizer to have more resolution and freedom in the shape creation.

Once the roll hoop will be mounted in the car's monocoque during the static test, the model is not constrained directly on its base nodes. Instead a 5.5mm thick layer of solid CHEXA elements is created in the base of the roll hoop as demonstrated in the figure 4.3, in order to simulate the monocoque's

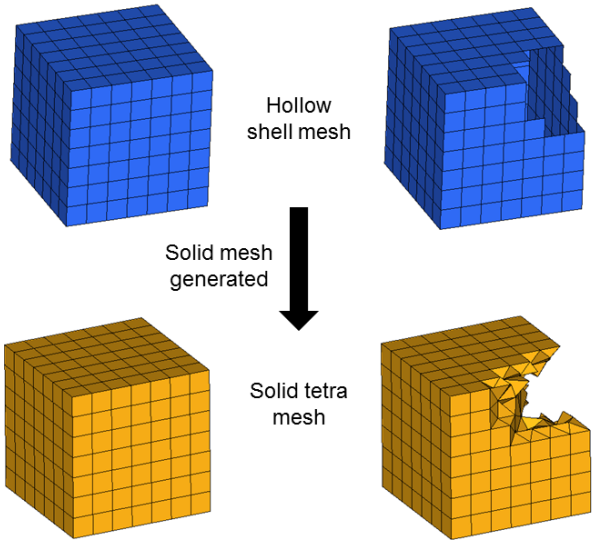


Figure 4.1: 3D mesh generation process.

stiffness. This layer is made of 0.5mm thick of ”bonding elements” and 5mm thick of ”aluminium elements”. The ”bonding elements” have the approximate stiffness of the bonding used to unify the two pieces together, and the ”aluminium elements” have the typical aluminium stiffness.

Is then in the base of this last elements that the model is constrained in the three translational degrees of freedom (x, y and z). This way the typical stress concentration near the constraints is absorbed by this bottom elements and the roll hoop's base is modeled a little bit closer to what would happen in reality.

The load application also deserves some attention once it might have a considerable impact on how the roll hoop behaves during loading. Ideally a contact analysis would be performed simulating the interaction between these two bodies. However contact analysis are computationally expensive and not so relevant for the initial iterations where we are more interested in defining an overall good shape and not so much in the contact area. For this reason, in this first iterations, the load is applied to an RBE element that is connected to the nodes of the roll hoop that would first contact the loading pad. In figures 4.2(b) and 4.2(c) this load application strategy is illustrated.

Once the global geometry definition is in a further developed stage, the geometric non linear analysis with contact interaction is performed.

Since 3mm thick rubber was allowed to be used between the roll hoop and the load pad, in this first iteration a 3mm layer of solid elements was extruded at the contact location of the roll hoop and pad as visible on figure 4.2. This not only applies the load offset caused by the rubber, as it avoids excessively stressed elements due to the RBE's rigidity in the roll hoop's body. Nevertheless, this method was only used in the optimization run since it was a more sensitive analysis. Later models do not include this extruded layer of elements.

To terminate this section the material properties used in the following iterations are described in the table 4.1. In the first 4 iterations it was not known the exact stiffness of the roll hoop's material; to overcome this drawback an approximate stiffness was used to model the material. However the material property update had no impact in the results.

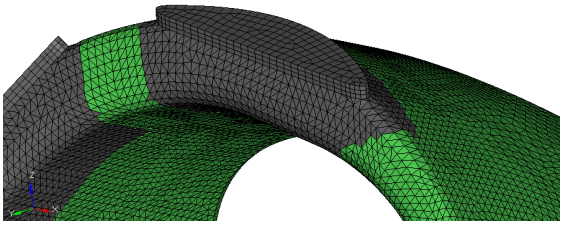

(a) Extruded elements

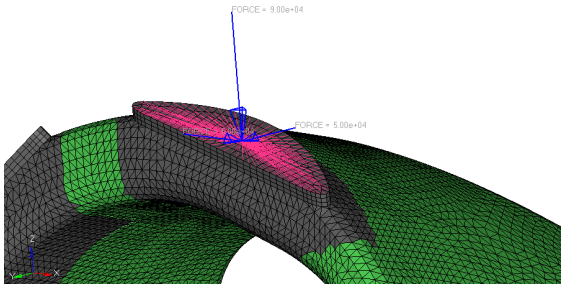

(b) Loading RBE and applied load

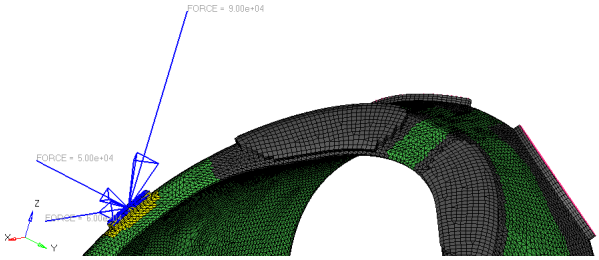

(c) Loading RBE at rear

Figure 4.2: Roll hoop mesh at loading locations.

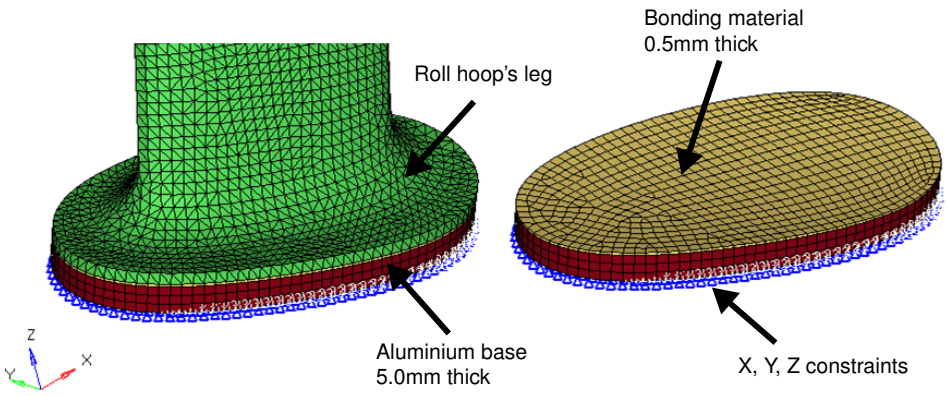


Figure 4.3: Roll hoop's supporting base.

| Material | Young Modulus [MPa] | Poisson's Ratio | Density [Kg/mm$^3$] |
|---|---|---|---|
| Generic Aluminium | 70 000 | 0.3 | 2.7x10$^{-6}$ |
| Generic Adhesive | 2 500 | 0.3 | - |
| Roll hoop's material | - | - | - |

Table 4.1: Material properties.

## 4.2 Iteration 1 - Topology Optimization

In this first iteration the topological optimization was performed in order to evidence the principal load path and reinforcements that should be done to the roll hoop. As said before the optimizer used is OptiStruct together with the RADIOSS solver.

### 4.2.1 Optimization Setup

Setting up the optimizer correctly is an important step to have good results. Here are described the values for the parameters that control the optimization process.

Concerning equation 3.1 the the penalization factor $p$ was set to 2, once it allows for good penalization of intermediate densities without over doing it. Is possible to make this values vary along iterations but in this case the value of $p$ was kept constant so that penalization was not to harsh.

Constraint screening parameters were kept as default once usually it outputs good results for the majority of the problems. Even if these values were to be changed, it would be preferable to first perform a standard analysis so that a better sensibility to the problem was obtained, and then try a new set up values in order to improve results. However even in default values OptiStruct outputs good results.

The objective function defined was to minimize the roll hoop's mass. Constraints were set as a maximum displacement of 20mm in the loaded nodes. Regulation impose a maximum deformation under loading of 25mm but, as precaution measure and in order not to get to close to this limit, 20mm is the maximum allowed in the optimization.

In figure 4.4 we have the roll hoop original shape just prior to run the optimization. The Design domain is limited to the green area. In other words only the green coloured elements will have a varying density attributed by the optimizer. The elements in grey and yellow colour are near the load application area or naturally tend to concentrate the loads. For this reason they are excluded from design space in order to guaranty the this region remains solid.

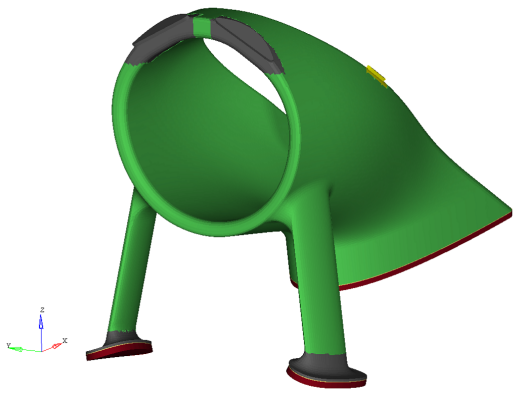

Figure 4.4: Roll hoop in original shape.

As in all sections from here on, the model is constrained as described in section 4.1, and is made of same material.

| Description | |
|---|---|
| Number of elements | 526 219 |
| Number of elements in the design space | 453 713 |
| Predominant type of element | CTETRA |
| Element size | 2mm |
| Optimization objective | Minimize mass |
| Optimization constraints | Maximum displacement of 20mm in loading nodes |
| Roll hoop's weight (from FE model) | 6.27Kg |

Table 4.2: Model information and optimization set up.

### 4.2.2 Optimization Results

In pictures 4.5 are presented the element density results from the optimization process. In blue are represented the elements with zero or near zero density, and in red the elements with density value of one.

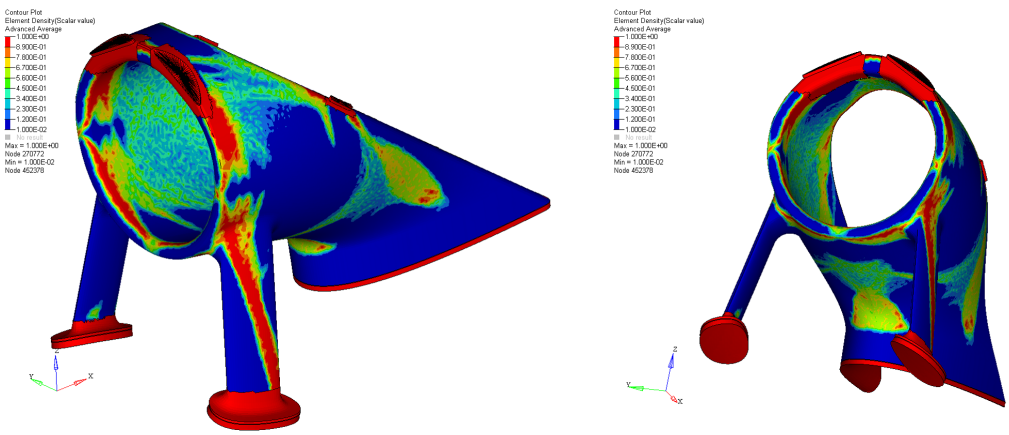


(a) View I (b) View II

Figure 4.5: Optimization output. Elements density.

If we hide the lowest density elements we obtain clearer image of the optimization results as shown in figure 4.6. From this figure is clear that a main load path begins to appear (highlighted in figure 4.7). The roll hoop's leading edge is practically solid, and the rear loading location is supported by an "oblique beam" that unifies the rear section of the roll hoop to the front where the legs take a big part of load.

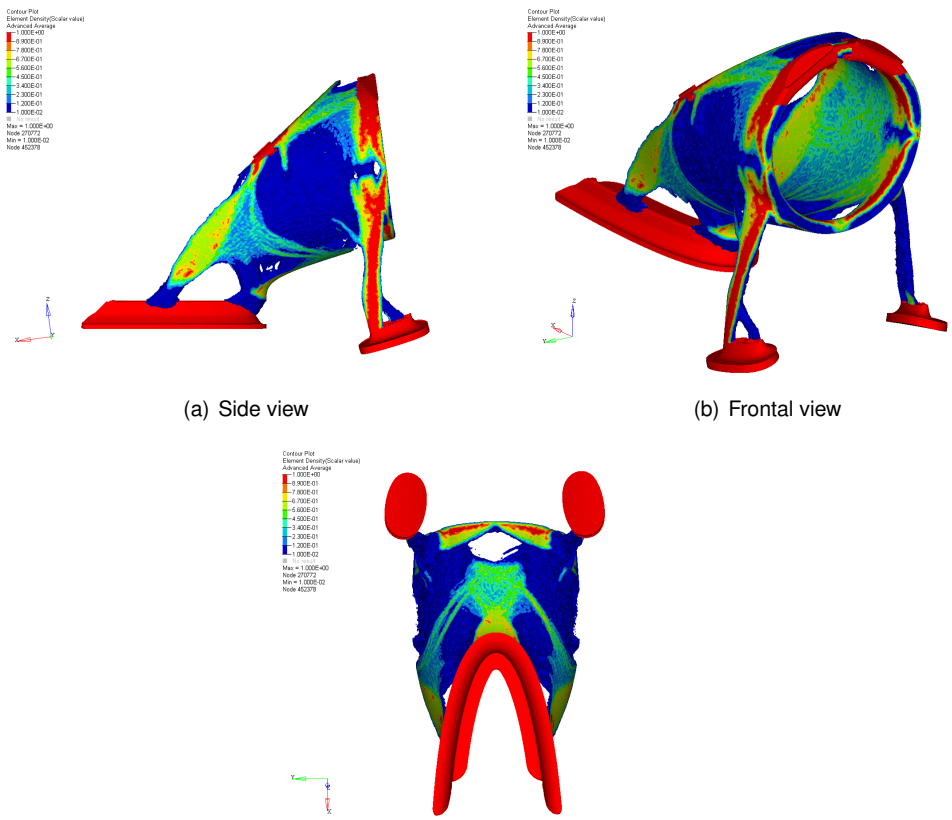


(a) Side view (b) Frontal view

(c) Bottom view

Figure 4.6: Optimization results. Elements density.

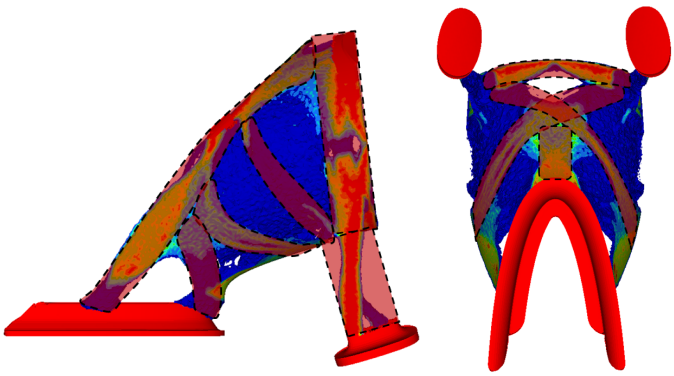

(a) Side view (b) Bottom view

Figure 4.7: Main load path.

However there are some considerations to account for and filter from this results. Once the optimization was done without buckling considerations, the front legs would easily buckle if it were made so thin (see figure 4.8). Besides, no material limit stress was imposed in the optimization set up which does not prevent the stresses from getting unrealistically high. However is preferable not to constraint the elements stresses once this usually causes hither convergence problems, or uninteresting results due to local stress concentrations (such as near RBE elements) or highly deformed elements that unknown to the user.

Is also important to notice some checkerboard elements in the roll hoop's inner skin as displayed in figure 4.8. This means that some of the load is still flowing through this location and thus some reinforcements should be placed in this area.

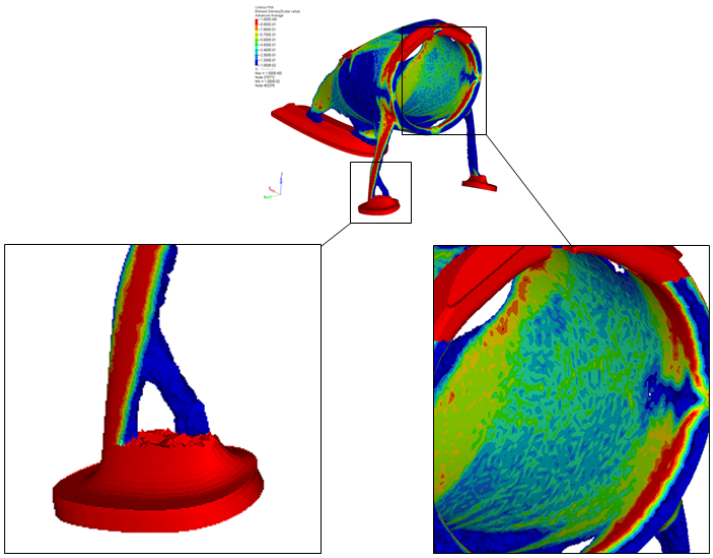

Figure 4.8: Checkerboard and buckling considerations.

Independently from some these imprecisions on the results from OptiStruct, is clearly possible to retain a geometric shape that both respects the optimization constraints and minimizes the mass of the piece. In the end experience and sensibility combined with the technical knowledge, should give the user of this commercial codes the capability to filter the most interesting shapes from this results and create an optimum or close optimum structure.

It was based on this results that the geometries from iteration 2 and beyond were generated.

## 4.3 Iteration 2 - Structural Linear Analysis

### 4.3.1 New Geometry Description

In iteration 2 the overall aspect of the roll hoop's geometry is visible in figure 4.9. The strategy adopted to create this geometry was to hollow the previous shape and add reinforcing ribs between the two skins. Afterwards holes were created in order to remove material. The legs were made hollow, creating a very large hole at the bottom of these that might cause problems when bonding it to the monocoque. However, this and other situations will be revised in the following iterations.

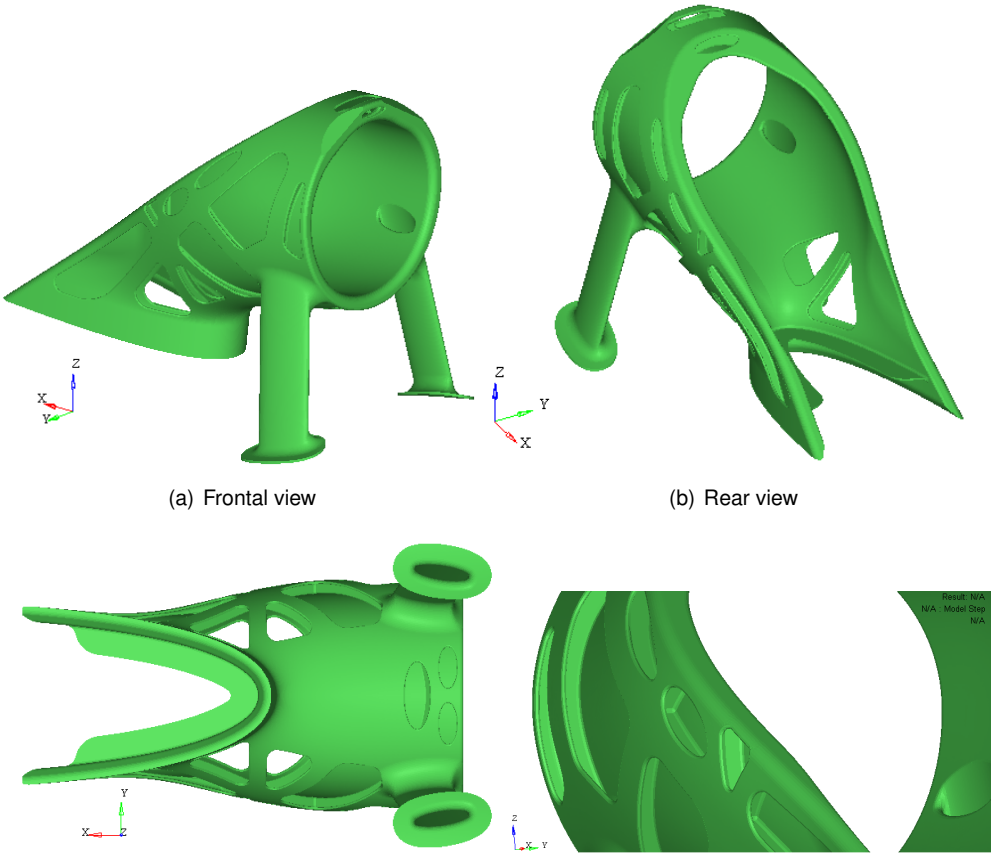


(a) Frontal view (b) Rear view

(c) Bottom view (d) Reinforcing ribs

Figure 4.9: Iteration 2 geometry.

In figure 4.10 are illustrated some of the most relevant dimensions for this new geometry as well as the previously referenced reinforcing ribs.

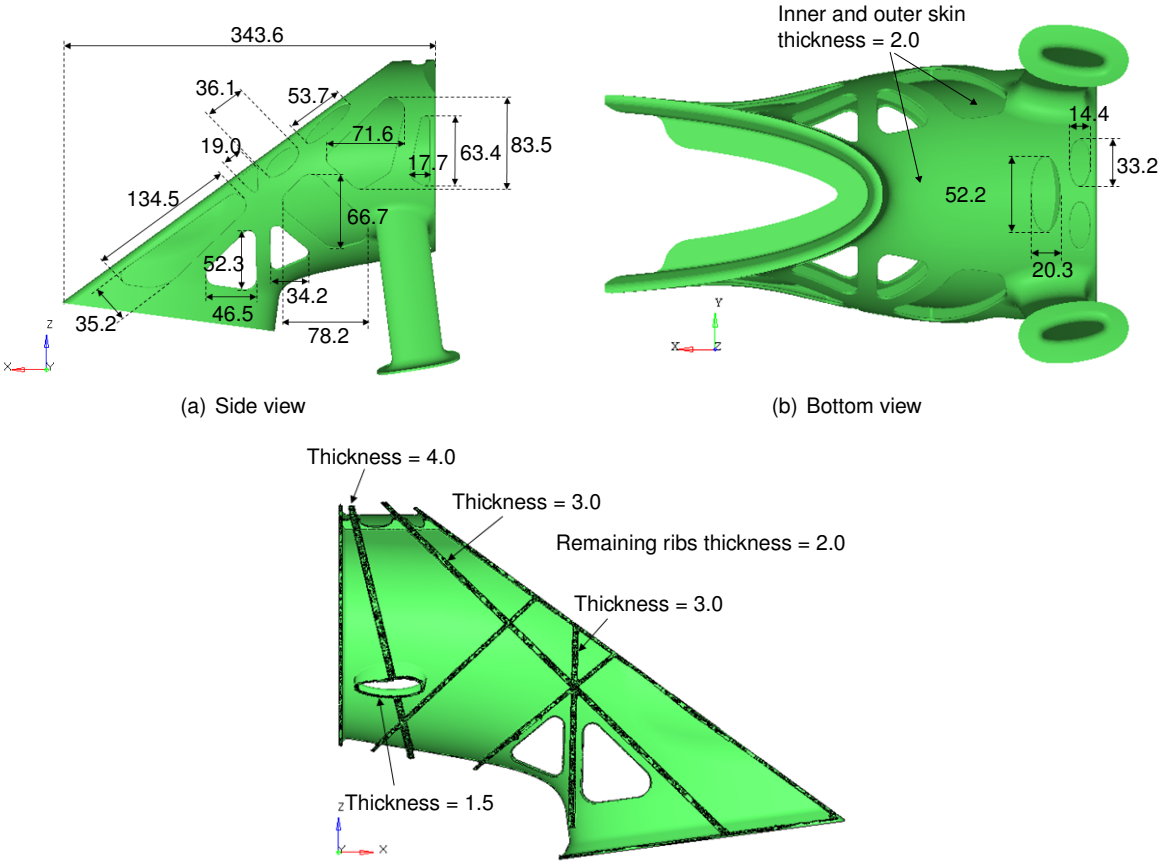


(a) Side view

(b) Bottom view

(c) Reinforcing ribs

Figure 4.10: Iteration 2 geometry dimensions (dimensions in mm).

### 4.3.2 Model and Results

Similarly to the model of the first iteration, the FE model used to study this geometry was made according to the directives described in section 4.1, apart from the element size that was reduced to 1mm. Once the geometry complexity is increasing and surfaces are getting thinner, the element size reduction seemed appropriate, not only because it allows a better stress distribution along the thickness of thicker sections, but also because it reduces the change of having excessively deformed elements. Table 4.3 resumes general characteristics of the model.

| Description | |
|---|---|
| Number of elements | 1 652 762 |
| Predominant type of element | CTETRA |
| Element size | 1mm |
| Roll hoop's weight (from FE model) | 2.16Kg |

Table 4.3: Iteration 2 model characteristics.

Figure 4.11 presents the von Mises stresses from the linear analyses performed to this geometry. We recall that the roll hoop must be tested for a given load applied in the forward and rearward direction (please see section 2.3). For this reason, the easier way of analyze the results from the two load cases,

is to combine them in one envelope that retrieves the worst stresses from both. This is demonstrated in figure 4.11(c).

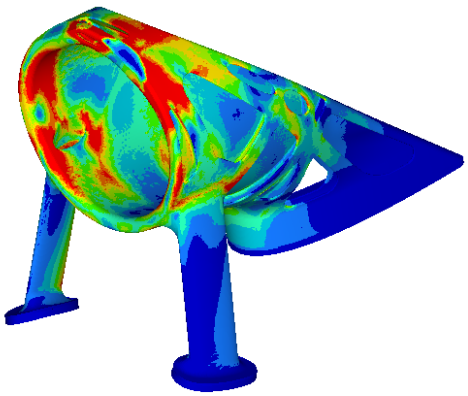

(a) Von Mises stresses for forward load load case.

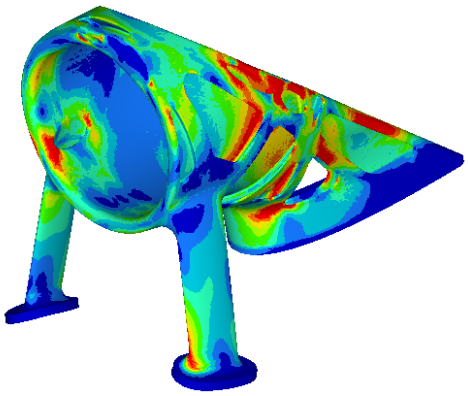

(b) Von Mises stresses for rearward load load case.

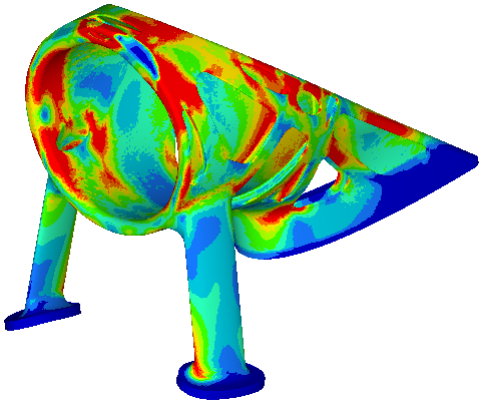

(c) Von Mises stresses envelope.

Figure 4.11: Iteration 2 results for forward and rearward load load cases.

In all figures where stresses are plotted, higher stresses are represented in red and the lower in blue. Also to notice, regions colored in red are beyond the material's yield stress and thus further measures must be taken. Although is desired to avoid material yielding, we will allow it to occur if it happens in small and local regions, and if does not reaches values too close to the material's ultimate strength.

Further detail from the analysis results can be seen in figures 4.12. Here we highlight several regions of the roll hoop under yielding that are of greater concern.

From this figures we can say that near the load application, is expected to always have material plasticity once the load concentration is to high. Nonetheless, plasticity should remain local and not endanger the surroundings.

In the roll hoop's leg there is also a large region of material under yield, and considering the importance of this component, is important to address this issue in the next iteration. The same is applied to the unions between the legs and the roll hoop's body.

As in the forward load situation, local plasticity on the load application region of the rearward load must be considered. However, at this stage the region under yield is larger than what we call acceptable, and measures must be taken for the next iteration.

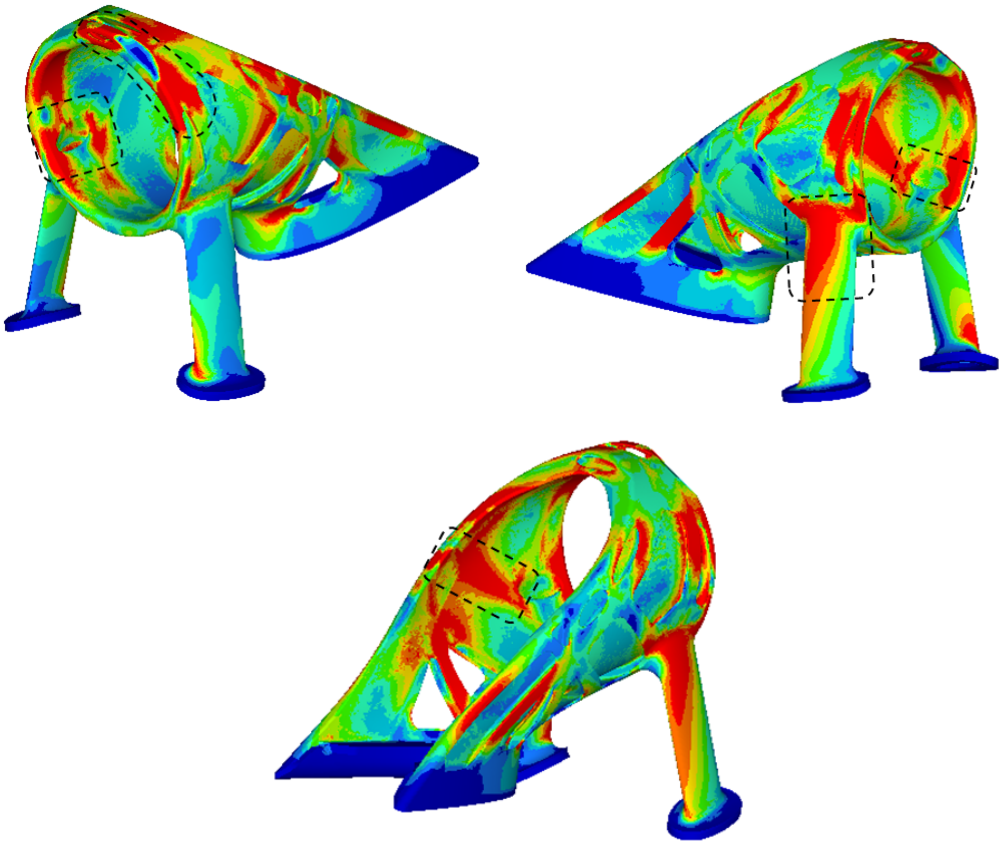

Figure 4.12: Von Mises stresses with areas of greater concern highlighted (load cases envelope).

Although the highly stressed regions, there are also low stressed areas where some material can be removed. These regions are evidenced in figure 4.13. The dark blue areas in the rear of the roll hoop will not suffer weight reduction modifications once they are connecting the piece to the monocoque. Thus it is required for current material to exist. Stresses in the elements of this area are reduced because they are close to constraints and thus do not deform much.

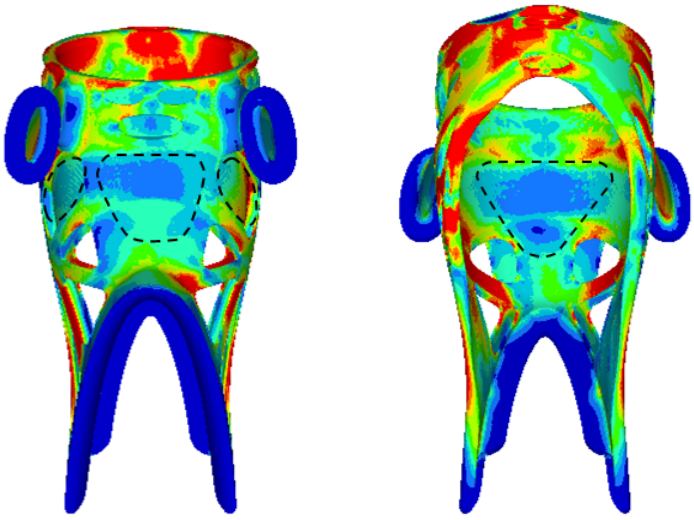

(a) Bottom view (b) Top view

Figure 4.13: Least stressed areas (load cases envelope).

Figure 4.14 shows a displacement plots, for both load cases, amplified by tree times. Maximum displacement is verified for the forward load load case with a value of 11.1mm. This value is well under the 25mm threshold established by the regulation (see subchapter 2.3).

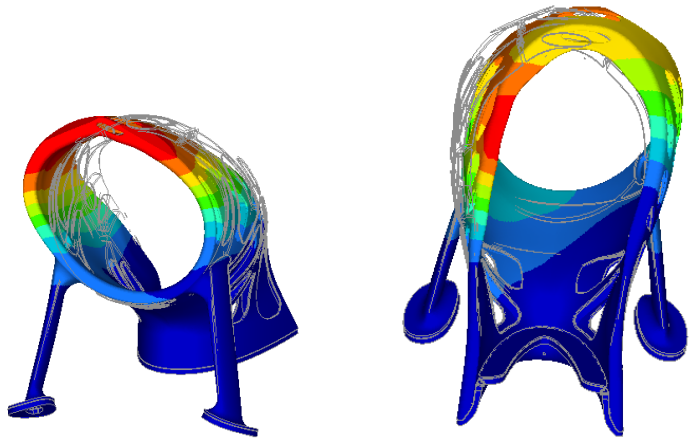

(a) Forward load load case. Maximum displacement of 11.1mm.

(b) Rearward load load case. Maximum displacement of 6.7mm

Figure 4.14: Load cases displacements. Deformations amplified 3 times.

Since this iteration presented interesting results, the following iterations will present similar geometries once were created from small modifications on the actual.

## 4.4 Iteration 3 - Structural Linear Analysis

### 4.4.1 New Geometry Description

In iteration 3 the principal changes in geometry were the resizing of some holes, the creation of new ones and the thickness change in several regions of the roll hoop in order to mitigate the severe yielding verified in the previous iteration. In figure 4.15 a side by side geometry comparison is made between iterations 2 and 3 in order to better understand the changes. In this figure we present the dimensions of the new holes, as well as the dimensional changes made to the previously existing ones.

The issue with the open hole at the leg's base was solved by an almost complete closure of this. The small hole left at the base of this is to allow the removal of the sintering powder that results from manufacturing process (see chapter 2.1).

The thickness changes relative to the previous iteration can be seen in figure 4.16 also in a side by side comparison. This is the most effective measure taken in order to reduce the excessively high stresses previously verified, once it considerably increases the section area of the affected regions and thus reducing the pressure (stress). Naturally, the biggest thickness increases were made in the areas of higher stresses. All the thicknesses were risen or maintained being the new holes the only weight reduction measure taken.

The area were the frontal load is applied has been made solid in order to better accommodate the

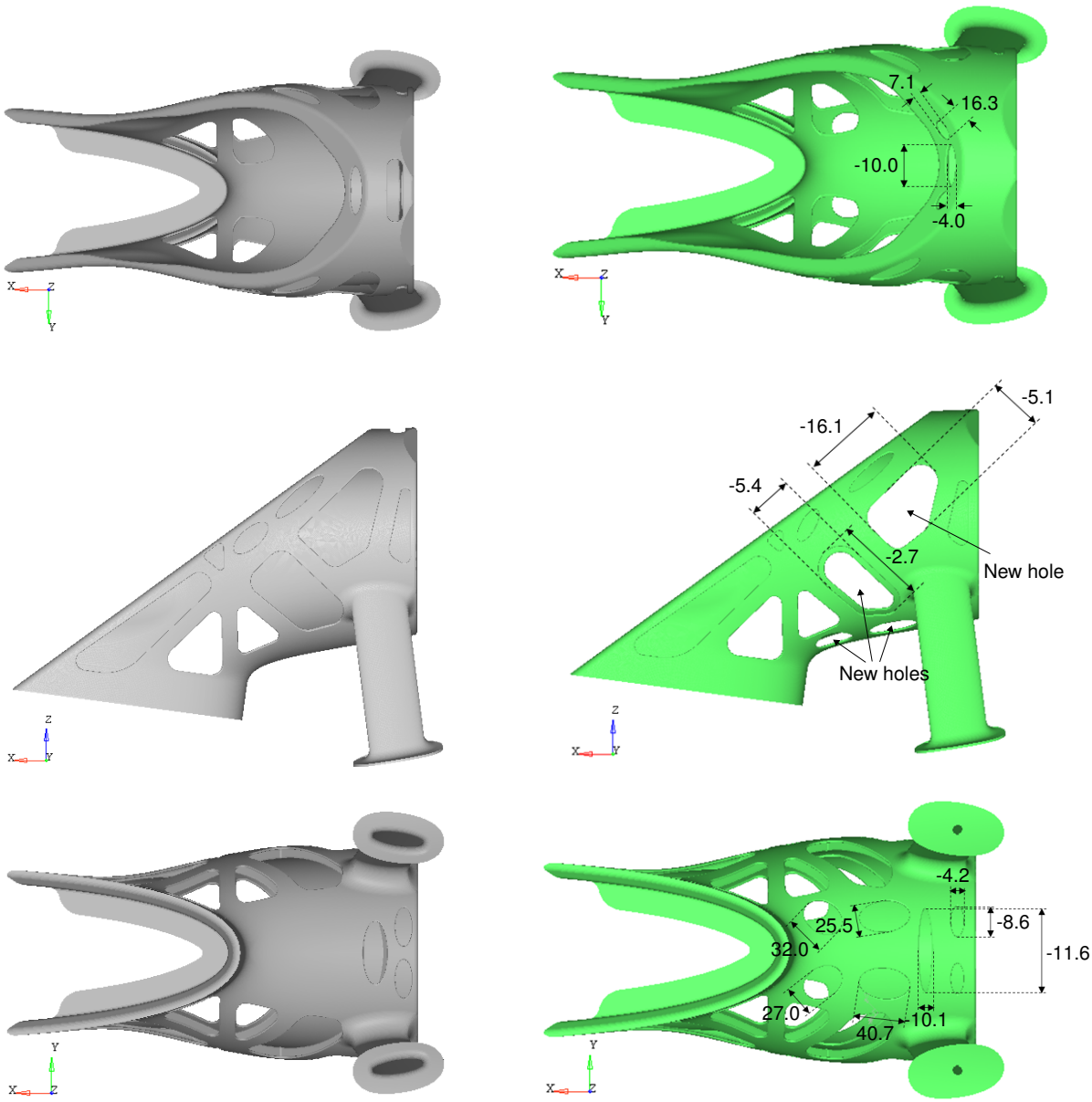


Figure 4.15: Geometry evolution between iterations 2 and 3 (dimensions in mm).

severe load applied in this region (see figure 4.17). Although this will not avoid material plasticity, it represents a considerable reinforcement that will seriously reduce the chances of material rupture in this area.

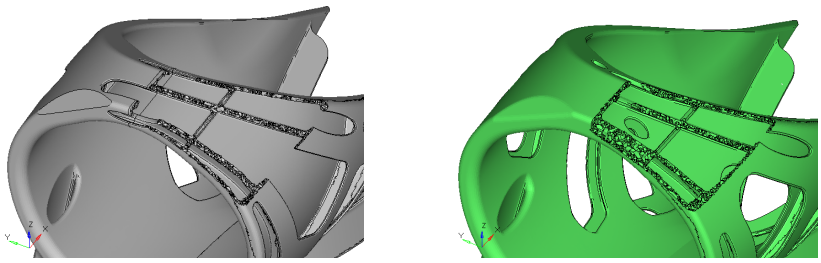

Figure 4.17: Solid reinforcement on load application area.

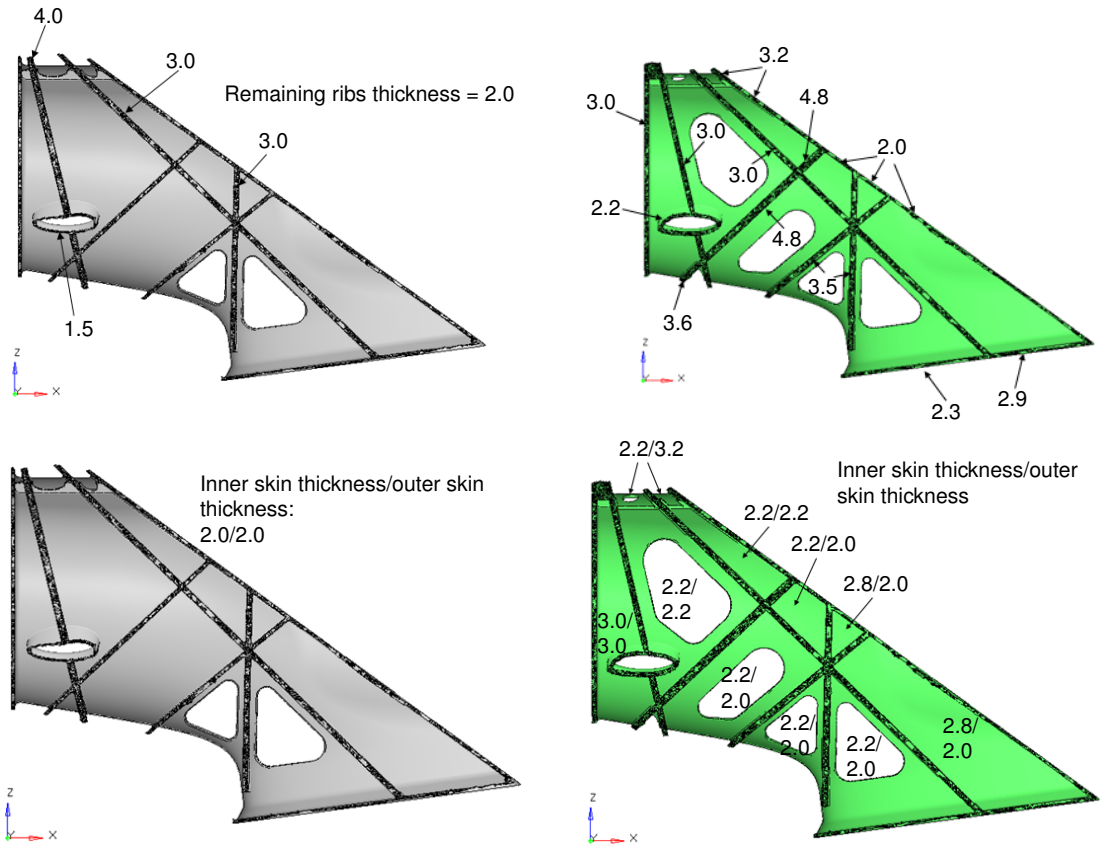


Figure 4.16: Skin and ribs thickness comparison between iteration 2 and 3 (dimensions in mm).

### 4.4.2 Model and Results

Due to its geometric similarities, the FE model for this iteration was done according to the same guide lines as the one of the previous iteration (see subchapter 4.3.2). The general characteristics of the current FE model can be seen in table 4.4.

| Description | |
|---|---|
| Number of elements | 2 109 249 |
| Predominant type of element | CTETRA |
| Element size | 1mm |
| Roll hoop's weight (from FE model) | 2.47Kg |

Table 4.4: Iteration 3 model characteristics.

To have a clearer idea of the improvements reached in the current iteration, in figure 4.18 is shown a von Mises stress comparison between iteration 2 and 3. As highlighted in this figure with a dashed line, the greater improvements were achieved in the roll hoop's leg (a), circular entrance laterals (b), union between the leg and roll hoop's body (c) and (e) and the load application area (d).

Improvements in the roll hoop's leg are considerable, but further work must be taken in order to reduce the stress levels in the union of this component with the rest of the roll hoop.

In the circular entrance laterals, improvements were detected but the yield stress barrier was still overtaken. However the region under yield is quite local and not of concern once the rib behind this area

is well bellow the yield threshold. From now, this situation will be considered as acceptable as long it happens under the same conditions.

A considerable progress was also achieved in the front loading area. Although there is room for improvement, this area will always suffer from material plasticity due to the highly concentrated load.

In the union between the leg and roll hoop body (areas identified as (c) and (e) in figure 4.18), a slight reduction in stress values was verified. However, considering the importance of this union, further stress reduction is mandatory in order to assure structural integrity.

In the remaining areas the stress distribution did not changed much. Although not so critical as the highlighted areas, in many of these locations the yield stress was undesirably overshoot by more than what could be called acceptable. To correct this situation further measures would be taken.

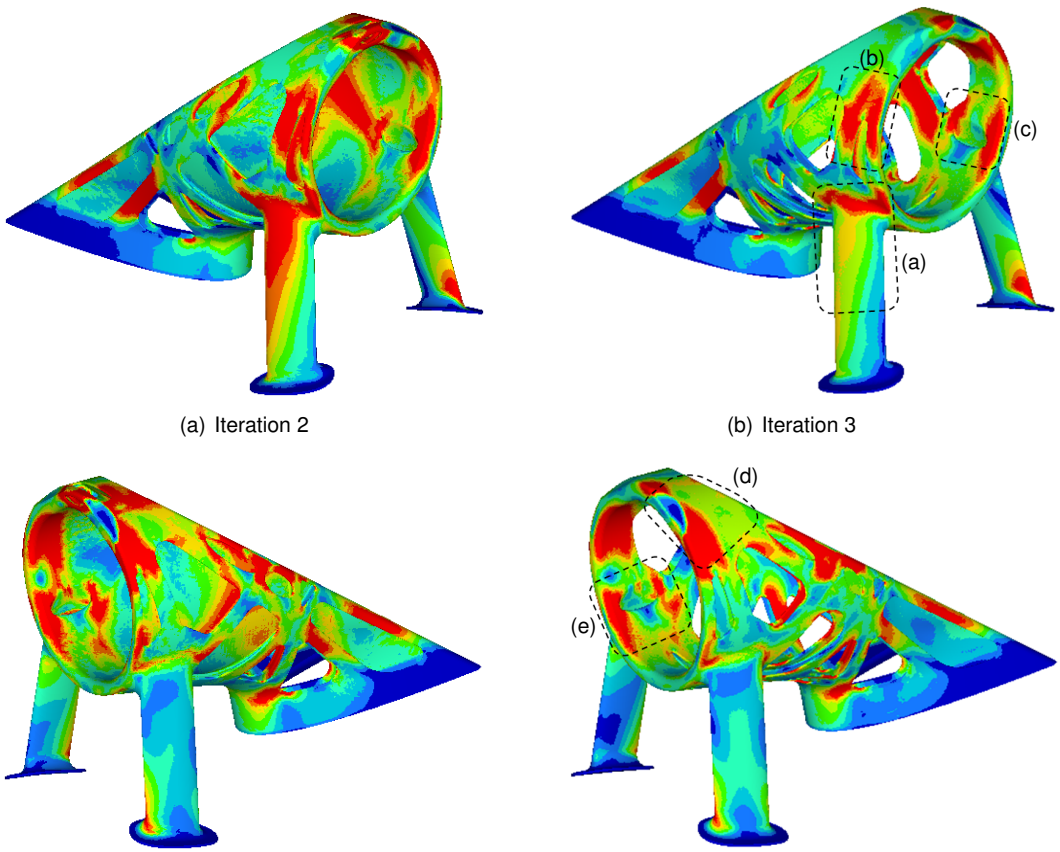


(a) Iteration 2 (b) Iteration 3

(c) Iteration 2 (d) Iteration 3

Figure 4.18: Von Mises stresses (load cases envelope).

Due to the reinforcements, the structure's stiffness increased and thus the maximum displacements decreased to a maximum of 9.1mm (11.1mm in previous iteration). A value well under the 25mm maximum established by technical regulations [5].

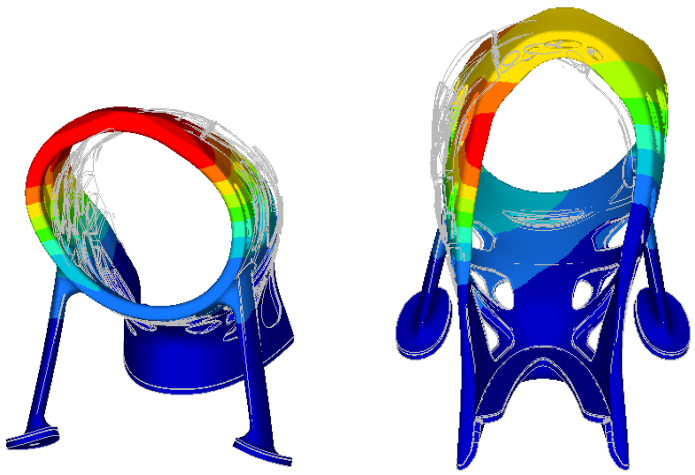

(a) Forward load load case. Maximum displacement of 9.1mm.

(b) Rearward load load case. Maximum displacement of 7.7mm

Figure 4.19: Load cases displacements. Deformations amplified 3 times.

## 4.5 Iteration 6 - Geometric Non-Linear Analysis with Contact Interaction and Material Plastic Behaviour

In this sub chapter we jump straight to the 6th and last iteration. In this iteration we approached our model closer to reality by introducing geometric non-linear effects, combined with material plastic behaviour and contact interaction between the roll hoop and the loading pad. Nonetheless a linear static analysis was also performed prior to this.

The procedure used through iterations 4 and 5 was the same used between iterations 2 and 3. In this iterations the modifications in the geometry were made with the goal of reducing the stress levels bellow the yield stress or to acceptable levels of plasticity, while using the minimum amount of material. Since the procedure used represented no novelty, these iterations are not documented here.

In this iteration is also evaluated the load case where the car is hoisted through the roll hoop. As already referenced in chapter 2.3, in some situations it might be necessary to hoist the car with a portable crane. Since the car's hoisting point is the roll hoop, this component must be evaluated for such situation.

A buckling analysis was also performed in this stage in order to evaluate the structure's stability when subjected to the loads imposed by the regulation.

### 4.5.1 New Geometry Description

In figures 4.20 and 4.21 we present a side by side comparison between the geometry of iteration 3 and 6. The major changes between these two are a new rib, thickness changes in the roll hoop's skin and legs.

The new rib is placed between the rear load application zone and the roll hoop's front section. This not only reinforces this area as it promotes a better distribution of the load applied in this section. While

in iteration 3 the majority of ribs had constant thicknesses, in iteration 6 almost all of the ribs vary their thickness along the length in order to optimize their strength and material distribution to the location requirements. This way the thickness increase in some ribs can be compensated by the reduction on some others, which helps keeping the weight low.

The outer and inner skin thicknesses were also revised in order to readapt to the stress levels verified in previous iterations. Due to the low stresses in this area, a new and large hole was created on the rear section of the inner skin, and the holes on the bottom section were redesigned according to the new ribs layout.

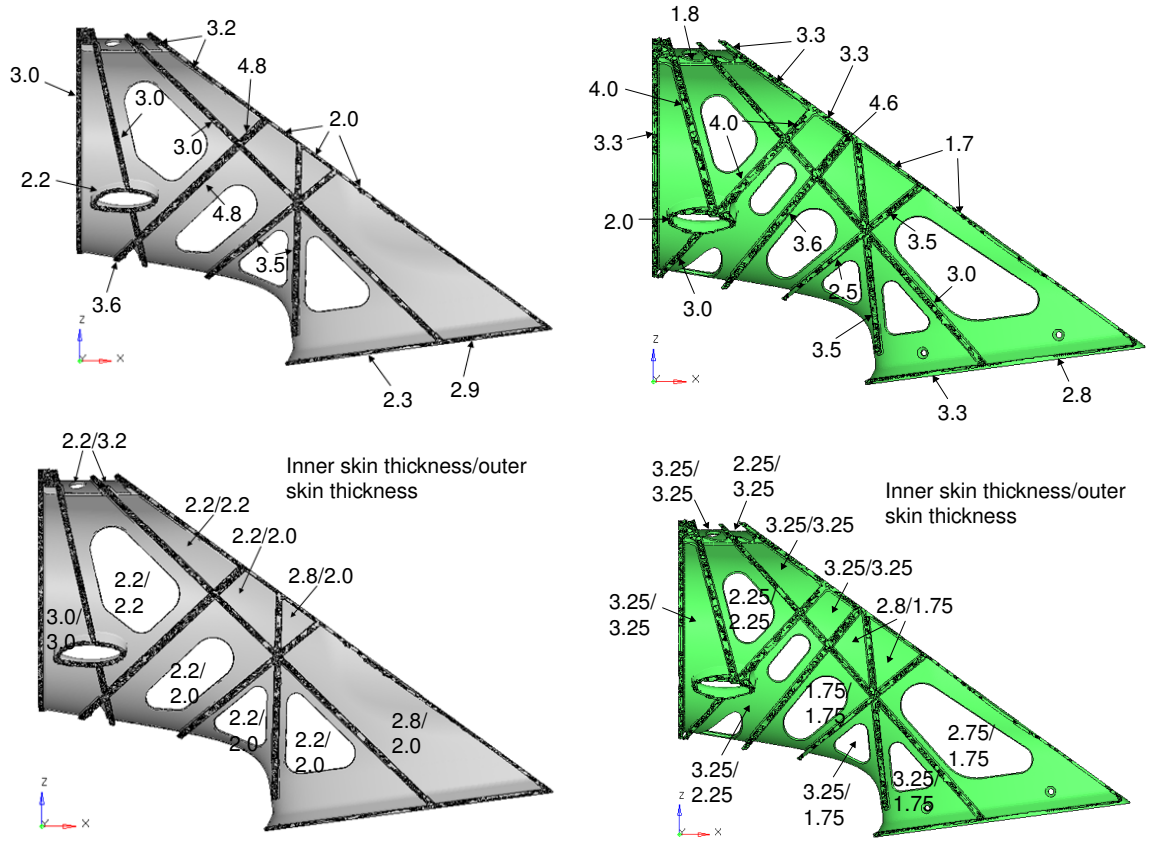


Figure 4.20: Skin and ribs thickness comparison between iteration 3 and 6 (dimensions in mm).

The fillet radius between the leg and the roll hoop's body (see figure 4.22(b)) was increased by 1.5mm to help reducing the stresses at this location.

According to the regulation is mandatory for all the cars to have several video cameras. On of them has to be installed on the top of the roll hoop, and hence the new circular shaped support on top of it (figure 4.22(a)). Since no major loads are expected to come from this camera no structural calculations were made to consider this element.

Since in this iteration the geometry is already in an advanced maturity stage, it makes scene to define the position of the fasteners holes once no major geometric changes are expected and stress levels are well known. We remind that the fasteners function is not to act a primary union between the roll hoop and the monocoque. Instead, they are used to make this union more robust in case the adhesive connecting the two parts fails unexpectedly during loading.

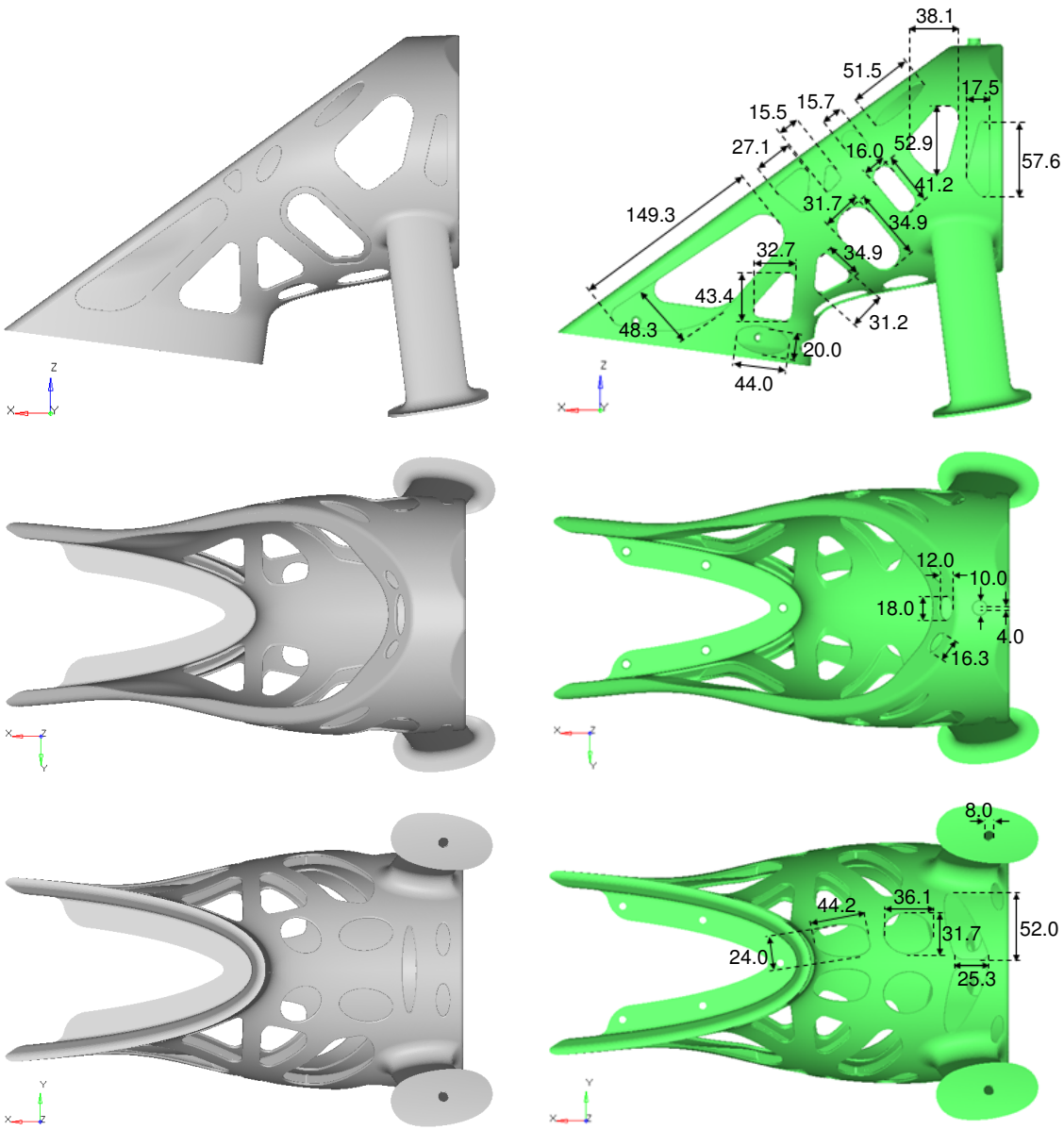


Figure 4.21: Geometry evolution between iterations 3 and 6 (dimensions in mm).

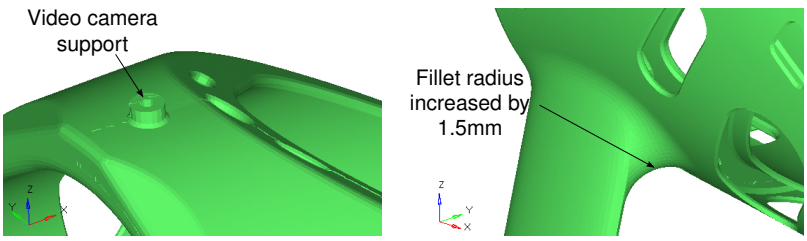


(a) Video camera support. (b) Fillet radius increase.

Figure 4.22: Video camera support and leg-roll hoop fillet details.

### 4.5.2 Model and Results for Linear Analysis

The model used in this iteration was made by the same guidelines as the previous ones. In this case the element size was slightly increased to 1.5mm instead of the traditional 1.0mm. This reduced the

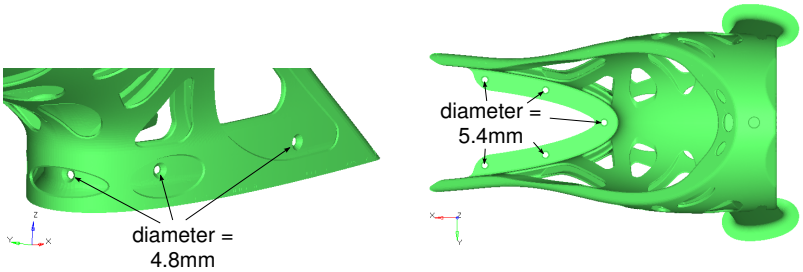


Figure 4.23: Holes for bolted unions.

number of elements through thickness of some areas, and thus the total number of elements. However the element density of the mesh remained good and produced good quality results. As usual the model general characteristics are resumed in table 4.5.

| Description | |
|---|---|
| Number of elements | 747 144 |
| Predominant type of element | CTETRA |
| Element size | 1.5mm |
| Roll hoop's weight (from FE model) | 2.51Kg |

Table 4.5: Iteration 6 model characteristics.

For the car hoisting load case the loads in the roll hoop are applied in a similar fashion to the regulation loads. The load is applied in the center of an RBE that is connected to the roll hoop nodes where is predicted to exist contact between the crane and the part. The load location and respective RBE's are displayed in figure 4.24. In reality the area of contact between the roll hoop and crane will be bigger than the one used by the RBEs, but using less area than reality makes this study conservative so the RBE's geometry will not be changed.

During hoisting, the car may have the tendency to till nose up or nose down. Depending on the situation the contact area in the roll hoop will be different, and for this reason, one RBE's is created for each situation. The hoisting load of 24.1 KN (see section 2.3) is applied in one of RBE at a time, and the two situations are computed on RADIOSS separately. While computing the nose up load case, the REB from the nose down load case is removed in order not to introduce artificial stiffness in the model and vice-versa. In figure 4.24 the arrow in red represents the nose up situation while the blue the nose down.

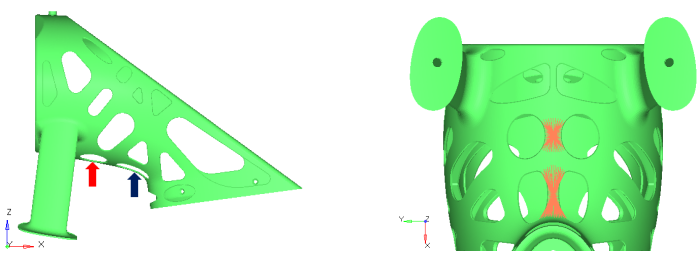

(a) Hoisting loads location. (b) RBE's for load application.

Figure 4.24: Model used for hoisting load case.

### Results for Regulation Loads

A linear static analysis made with this geometry revealed a considerable improvement relative to iteration 3. Material plasticity still occurs, but now affects smaller areas and the stress levels are lower than before. Figure 4.25 presents the results from this analysis and identifies the areas of greater concern.

As said before in iteration 3, the areas identified with (a) in figure 4.25 are near the load application area. As a result there is a severe load concentration in this area that makes it very hard to avoid plasticity. Nonetheless the yielding verified here is considered acceptable.

The situation in areas (b1) and (b2) remains acceptable since is in the same conditions as reported in subsection 4.4.2.

Region (d) is in similar conditions as (b1) and (b2). Yield stress is overshoot essentially in the inner skin but the ribs underneath it remain above this threshold.

Areas (c) and (e) are stress concentration points that tend to create stresses higher than desired due to its geometry. Even when more material is added (as in this case), there is still a considerable stress concentration in the areas of sharper angles. Considering the importance of this area this stress concentration is inconvenient, and the most efficient way to eliminate this problem is by locally changing the roll hoop geometry. Further ahead a brief study on a geometry change in this location is presented.

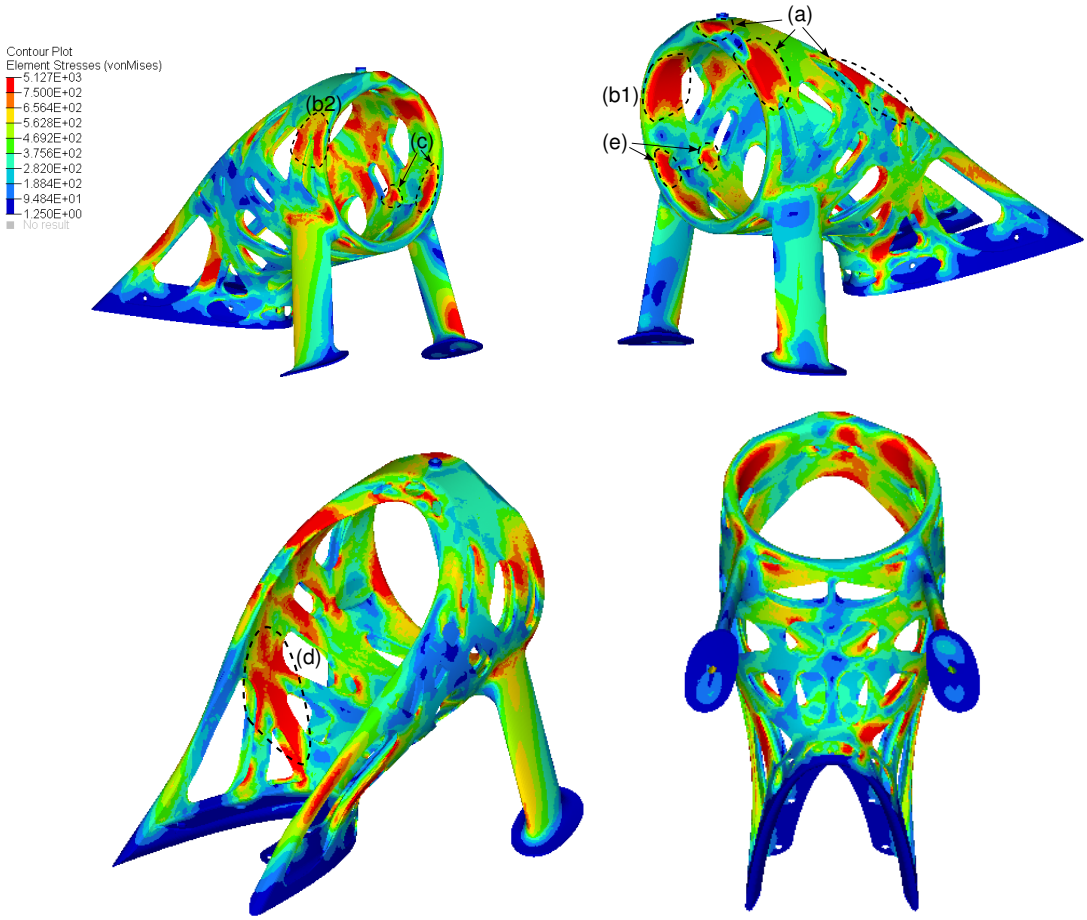


Figure 4.25: Von Mises stresses (load cases envelope).

The bond layer unifying the roll hoop to the monocoque also deserves some attention in this study

and for this reason a Von Mises stress plot is represented in figure 4.26. The peak stress registered in the bond layer is 139MPa but the allowable for this material is only 30MPa. However since the areas in failure are only under compression, this values do not represent a serious problem once the roll hoop will still have the support of the monocoque if the bond fails. In addition to this, the roll hoop is also bolted to the monocoque to strengthen the union for situations like this. As a conservative approach the bolted unions have not been simulated in this run since these would carry part of the load of the bond layer. So in reality the stresses in the bond layer will be lower than the ones here predicted.

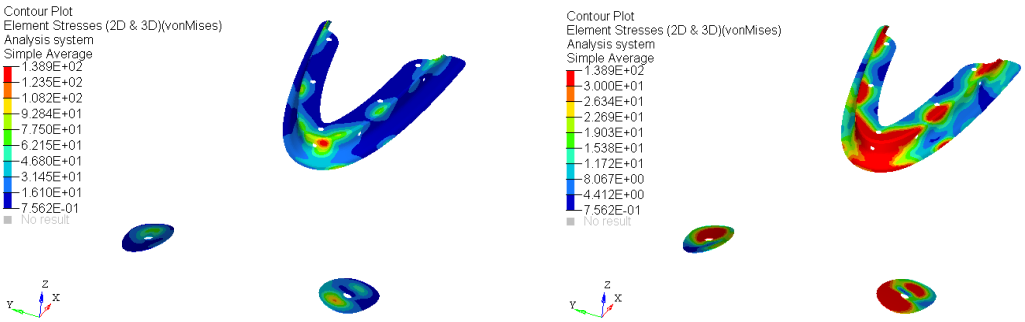


(a) Von Misses stress plot.

(b) Von Misses stresses above 30MPa are represented in red.

Figure 4.26: Von Mises stresses for the bond layer (load cases envelope).

### Hoisting Loads Results

The result from the hoisting load case are shown in figure 4.27. The stress scale is the same as used for all the other stresses plots. From this images we can say that the roll hoop is perfectly capable of withstanding these loads, since the only reasonably high stresses are the ones coming from elements near the RBEs. Since rigid elements have the tendency to create unrealistically high stresses near their surroundings, these will be ignored.

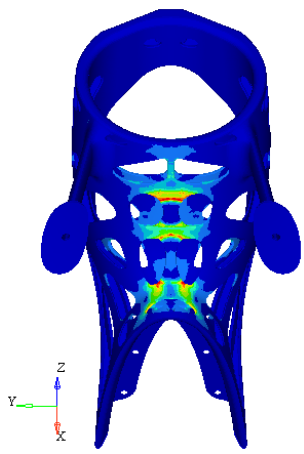

Figure 4.27: Von Mises stresses (nose up and nose down envelope).

**Bucking Results**

The results from the buckling analysis revealed to be quite positive once instability happens for a load 2.55 times the current load. The legs were the zone of greater concern due to their thin skin and crucial function, however the area most likely to buckle revealed to be in the rear as figure 4.28 demonstrates.

Table 4.6 resumes five of the absolute lowest eigenvalues obtained from the buckling analysis.

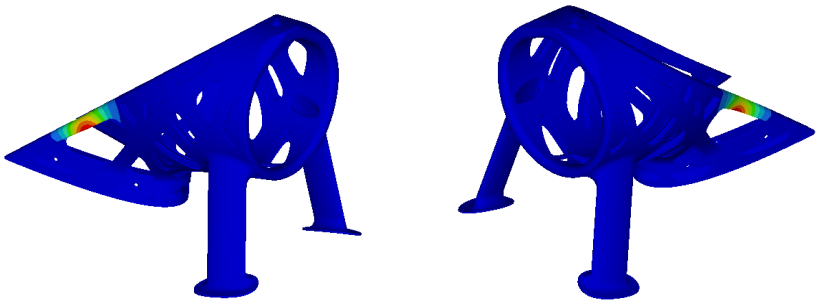

(a) First buckling mode for forward load.

(b) First buckling mode for rearward load.

Figure 4.28: Displacement plot for buckling results.

| Eigenvalue | Load Case |
|---|---|
| 2.55 | Forward load |
| -3.54 | Rearward load |
| 3.74 | Forward load |
| -4.94 | Rearward load |
| 5.44 | Rearward load |

Table 4.6: Eigenvalues from buckling analysis.

According to the analysis, buckling on the legs occurs if the forward load is 6.57 times bigger than what it is now.

### 4.5.3 Model and Results for Geometric Non-Linear Analysis With Material Plastic Behaviour and Contact Interaction

The model used for to run the non-linear analysis is the same as the one used for the linear analysis, apart from two circular loading pads of 50mm thick and 200mm in diameter. These are used to simulate the steel loading pads used in the real testes. Figure 4.29 shows the loading pads location and the areas of the roll hoop defined as the slave surfaces. This time, the loads are applied in the center of the loading pads that can not rotate, and only move along the load direction.

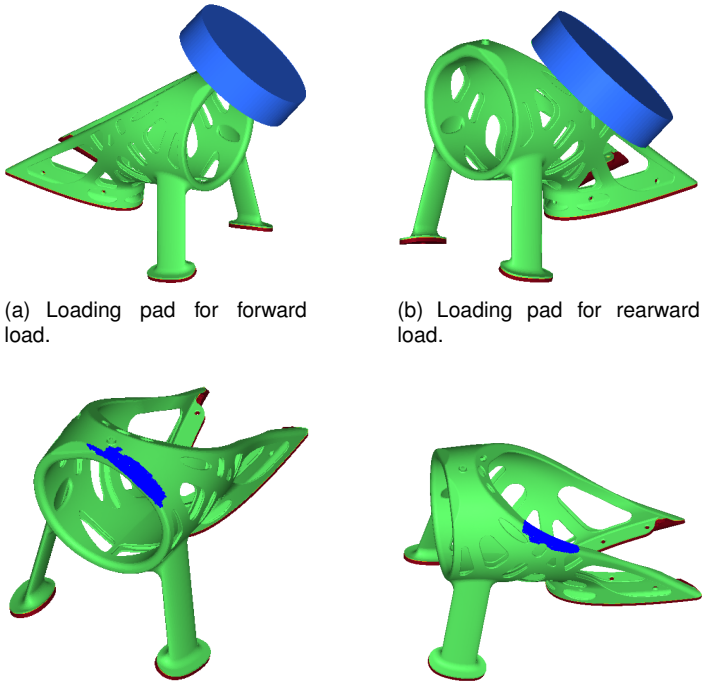

(a) Loading pad for forward load.

(b) Loading pad for rearward load.

(c) Slave surface for forward load.

(d) Slave surface for rearward load.

Figure 4.29: Model for non-linear analysis.

Since we are now considering the non-linear material behaviour, in this run the material has been modeled as a perfect plastic behaviour. This means that the stress/strain curve is assumed linear until the yield stress, and horizontal from this point on. In other words, once the yield stress is reached, the stresses do not increase any more with the strain. This way an element under yielding does not ”absorb” any more load, forcing this to be redistributed to the surroundings.

To model the contact between the roll hoop and loading pad the contact discretization chosen was node-to-surface. We reckon both node-to-surface or surface-to-surface discretization approaches would generate trustworthy results considering the refinement of the slave surface (roll hoop). Thus, since node-to-surface has the tendency to produce higher peak stresses (more conservative) and is slightly cheaper from the computational cost point of view, this was the discretization method chosen.

Considering the characteristics of our problem we can say that no major sliding is expected between the slave and master surfaces. Besides these are parallel to each other and the local tangent plane is a good approximation of the master surface once this is flat and very rigid (not expected to deform much under loading). Thus, considering these facts, the tracking approach better suited and also chosen for this problem was small-sliding.

#### Results for Regulation Loads

The results from this analysis are shown in figure 4.30. As it would be expected, plasticity areas are now larger than the ones obtained with the linear analysis, once we are considering geometric non-linear effects and a different material behaviour. As a result from the contact modulation, is clear that both the front and rear loading areas (a) are now under higher stresses once the load is now applied by the

loading pad instead of an RBE. Due to its rigidity the RBE does not allow for the nodes of the elements connected to it to expand or contract. As a consequence these elements do not output stresses, which is incorrect. Nonetheless the stress level is not dramatically higher than in previous analysis, and thus this result is still acceptable.

Area (d) is the region were the stress levels registered the biggest increase. In the the outer skin several small areas are now is the plasticity region, but their small size does not represent a threat to the structural integrity of the roll hoop. In the inner skin however, the areas with the stress level higher than the material's yield value are bigger and more threatening. But a more careful inspection reveals than the ribs behind this region remain in healthy levels of stress, which gives us the confidence to accept the results.

On region (b) the situation remains essentially in the same conditions as in the linear analysis, and thus no further modifications are required in this area.

The results for the areas (c) and (e) revealed very similar to the linear analysis so the considerations to be taken area the same as before.

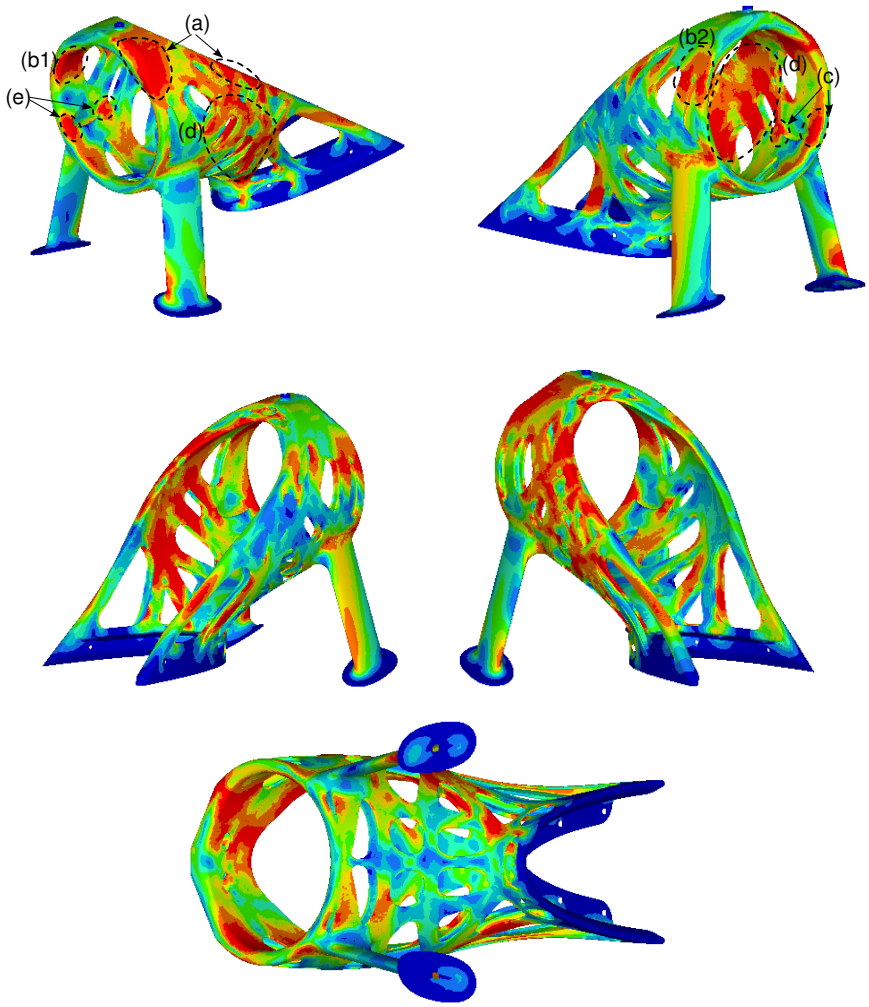


Figure 4.30: Von Mises stresses for geometric non-linear analysis (load cases envelope).

To have a better perception of the level of material plasticity, figure 4.32 plots the maximum principal

plastic strains for the two most critical load cases. Areas in blue represent 0% plastic strains and the element with the highest strain is plotted in red with a value of 14.5%. The material from which the roll hoop is made registered a minimum elongation at break of 15.6% for a small test campaign made with 3 sample coupons. The other two coupons registered a value of 18.3% and 18.4%, but as a conservative approach, the values of 15.6% will be used as a material ultimate strength reference value.

Although 14.5% is strain value dangerously close to the materials limit, this value was only registered on only 2 or 3 elements that have strangely high strain values relatively to their neighbor elements (see picture 4.31). This indicates that such high strain is unrealistic once such concentration was probably caused by a localized load peak or a particularly deformed element.

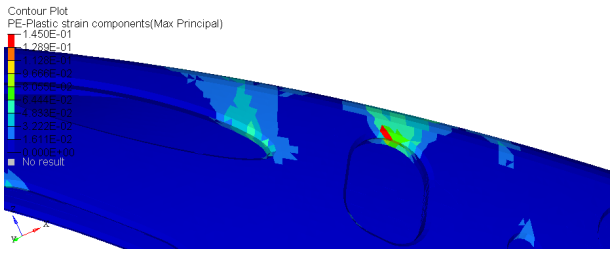


Figure 4.31: Unrealistic hight strains due to excessively deformed element.

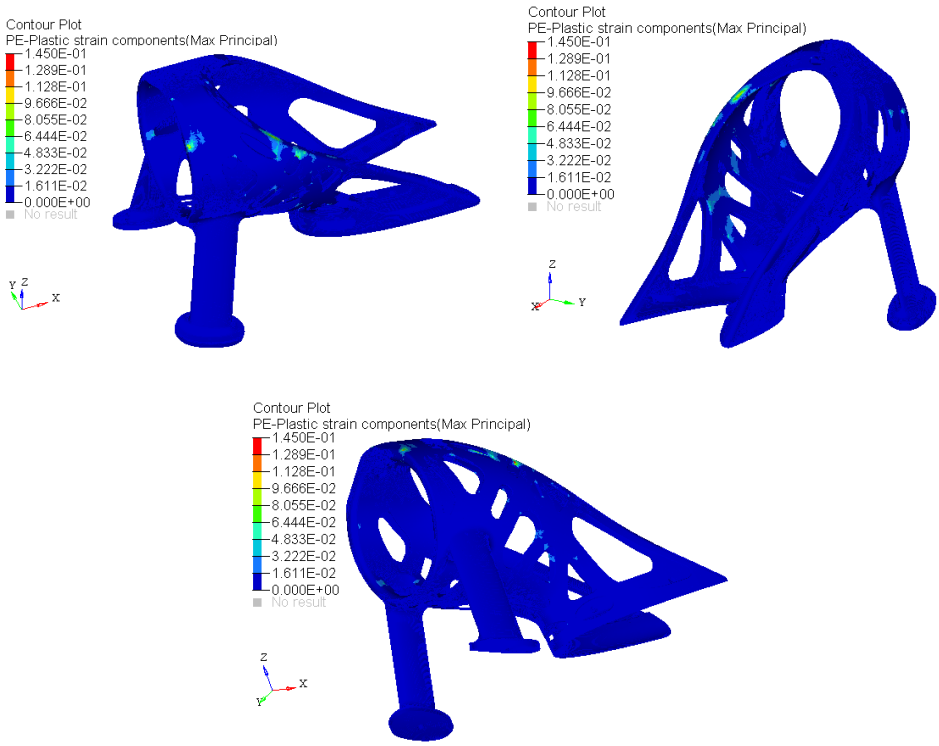


Figure 4.32: Maximum principal plastic strains. Load cases envelope for geometric non-linear analysis.

The more realistic maximum strain detected in this plots are values rounding the 12-13% in small areas near the load application points. Regions of greater concern, such as (c) and (e) from figure 4.30, have plastic strain rounding the 6-8% which is still considerably less than 15.6% allowable.

Concerning the bond layer, the non-linear effects resulted in slight increase of the maximum stress

to 140.8MPa. However, in figure 4.33(b) we can see that the area of bond layer with stresses above the 30MPa is smaller when compared to the linear static analysis (figure 4.26(b)). Thus, this small increase in stress can be neglected when compared to the overall stress reduction. Having said this and considering the facts about the bond layer referenced in subsection 4.5.2, we consider this results as acceptable

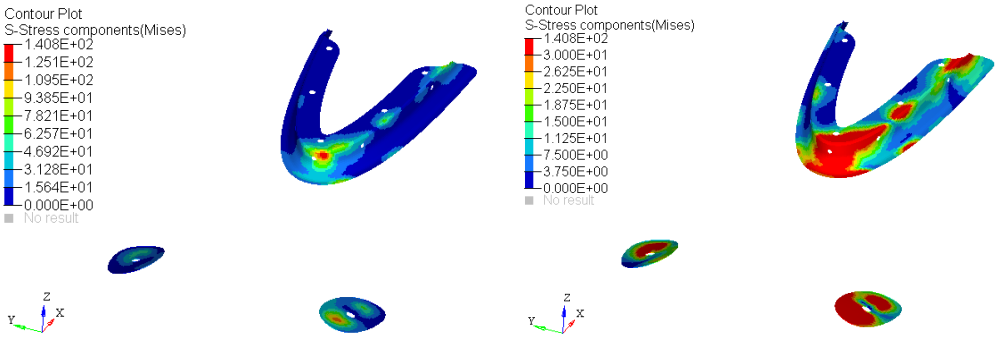


(a) Von Misses stress plot.

(b) Von Misses stresses above 30MPa represented in red.

Figure 4.33: Von Mises stresses for the bond layer (load cases envelope).

# Chapter 5

# Testing and Results

In this chapter we present the results from the static tests made to the roll hoop in order to certify it for competition. We remind that the tests must be performed with the roll hoop mounted on the survival cell and the total load of 119.2KN (50kN laterally, 60kN longitudinally in a rearward direction and 90kN vertically in downwards direction) must be applied to the roll hoop. For this test to be valid the load must be applied in less than 3 minutes and maintained for 10 seconds. The maximum deformation of the roll hoop must be less than 25mm under loading and structural failure is limited to 100mm bellow the top of the structure measured vertically.

Unfortunately the roll hoop did not pass the test at the first attempt due to a manufacturing defect. Thus in the following are explained the several attempts that were required to pass this test.

The necessary apparatus to make the test can be seen in figure 5.1, and figure 5.2 shows the first of two roll hoops as they come out of 3D printing. From figure 5.2 we can see that the roll hoop had to be printed in 5 separate parts since it did not fit as one piece in the 3D printer. This was a manufacturing constraint unknown to us at the time, and since the welding process weakens the alloy locally, special care must be taken so that the welding is not placed at locations of high stresses. Fortunately this was considered and the welds are far from the these regions.

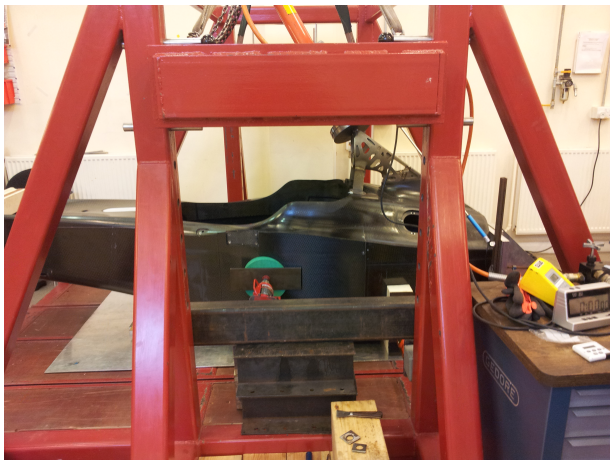

Figure 5.1: Static test apparatus.

## 5.1 First Attempt

Unfortunately an defect during the manufacturing process of the first roll hoop resulted in significant dent on the roll hoop's leading edge. The results from this faulty process are shown in figure 5.2 were approximately 1mm of material is missing near one the most critical areas of the roll hoop.

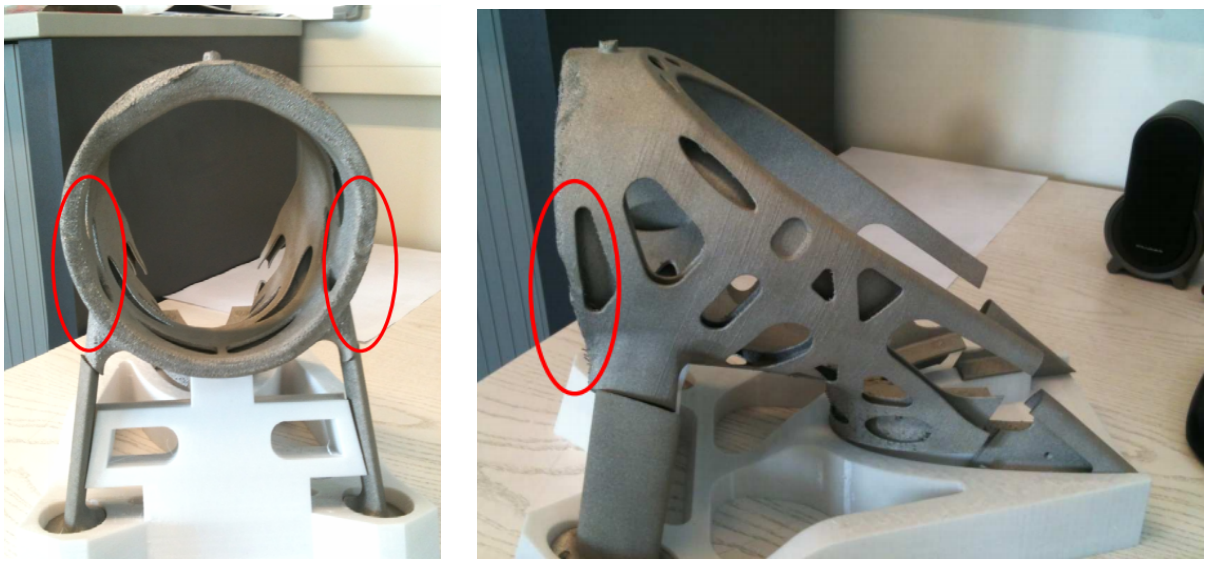

Figure 5.2: Dented roll hoop.

As a result from this imperfection the roll hoop failed the required test for a load of 116KN out of 119KN (97.5% of the total load), and two cracks opened in the area where the stresses were known to be higher (see figure 5.3).

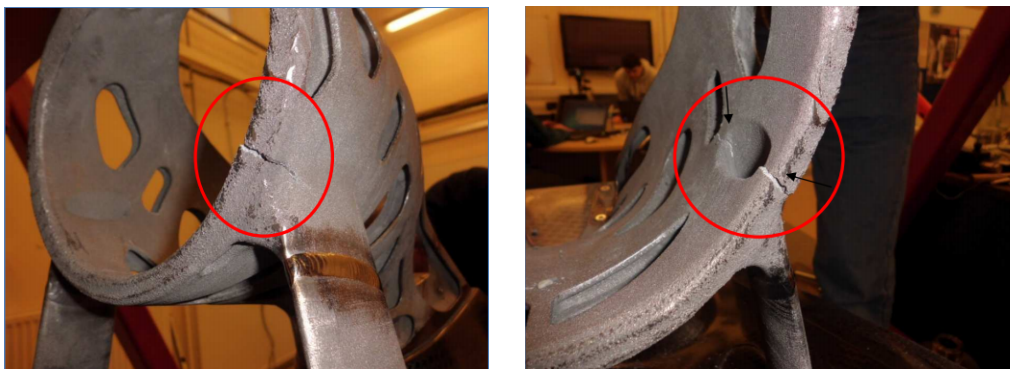

Figure 5.3: Cracks formed during testing.

## 5.2 Second Attempt

Faced with this problem, a repair was urgent in order to approve the roll hoop for competition. At the time, covering the top of the roll hoop's leg by welding a thin patch of material seemed to be the best solution. So with this idea in mind the FE model from iteration 6 was modified in order to simulate this

repair and evaluate its viability.

### Structural Linear Analysis of First Repair

To simulate the repair, a layer of shell elements with a thickness of 2mm was added to the FE model from iteration 6 in the area were the patch was going to welded (figure 5.4). In a normal situation a new FEM would be created from a new CAD model, but since we were in tight schedule and the repair consisted on a thin layer of material that can be accurately modeled with shell elements, this procedure was adopted.

Only a linear static analysis was ran since it is enough to evaluate the effect of the repair. The results from this analysis can be seen in figure 5.5 where a Von Mises stress comparison between the result from iteration 6 and this repair is presented. From this figure is clear that the stress reduction in this area is such, that the plasticity issues no longer exist. Which is a very important factor to consider, since the welding processes weakens the strength of the alloy. knowing that this improvement comes at a weight increase of 16g, this solution seemed appropriate and it was decided to advance with the repair.

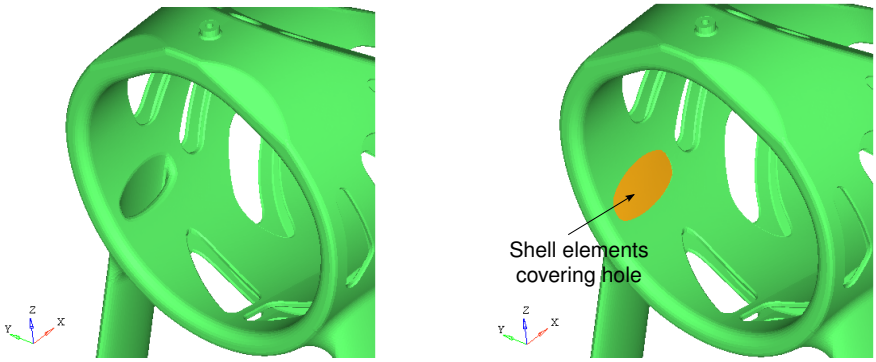


(a) FEM from iteration 6 (b) FEM from iteration 6.1

Figure 5.4: Iteration 6 and 6.1 FEM comparison.

Since this formula one team was competing with two cars the second roll hoop, with no imperfections, was rushed out of production and a patch welded in the vicinity of the original failure location, with the objective of increasing the local strength and create the geometry from figure 5.4(b). This proved to be a bad decision, as the weld was not as robust as it should have been and led to a failure at even lower loads (90 kN), right in the middle of the weld as shown in figure 5.6.

## 5.3 Third Attempt

At this point was mandatory for the roll hoop to pass the static test since another failure could jeopardize the participation of the team in the 2012 Formula One championship. Thus it was decided to make a more drastic repair.

This time, the leading edge of the roll hoop was saw and a solid ring of material was welded in its place, which resulted in the geometry from figure 5.7. To have a better perception of how big this

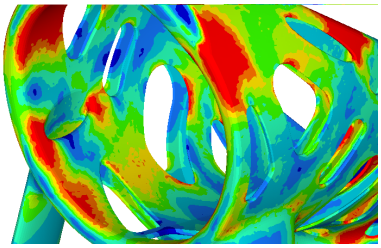

(a) Model from iteration 6

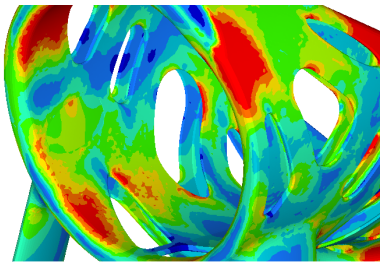

(b) Model from iteration 6.1

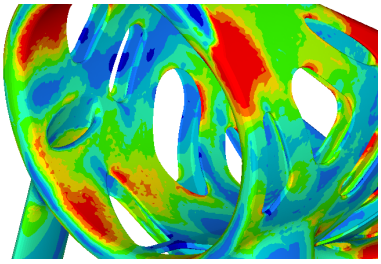

(c) Model from iteration 6.1 (shell elements hidden)

Figure 5.5: Von Mises stress comparison between iteration 6 and 6.1 (load cases envelope).

Figure 5.6: Crack created during the second attempt.

reinforcing ring is, figure 5.8 presents the section increase in the lower area of the leading edge. To handle better with bending, in the middle of the ring (half way between the bottom and top of the ring) the section is even bigger as it measures 26.9x15.0mm instead of 17.0x15.0mm.

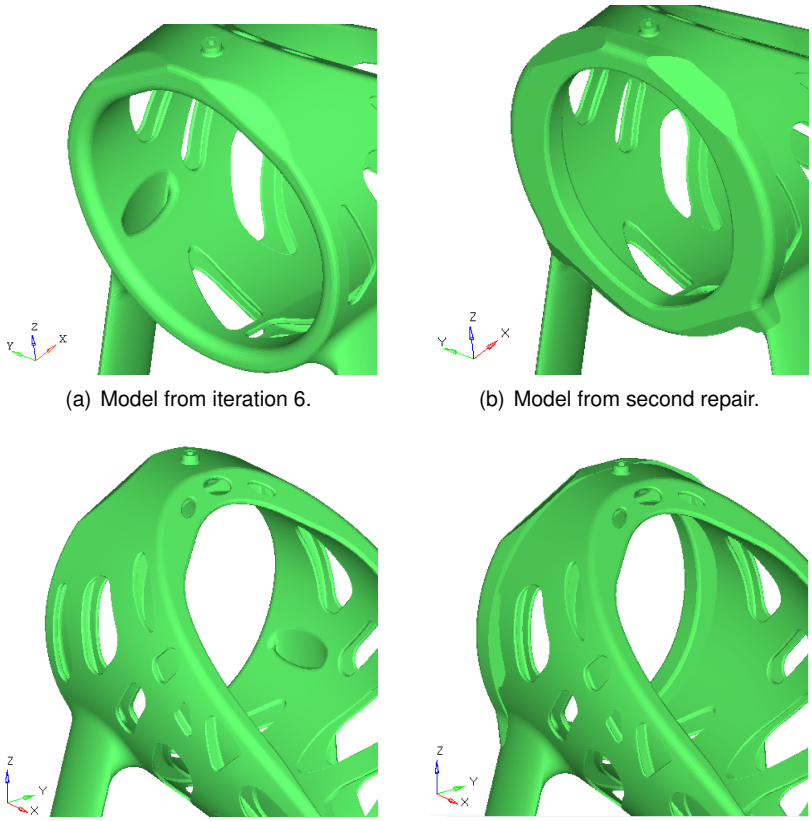

(a) Model from iteration 6.

(b) Model from second repair.

(c) Model from iteration 6.

(d) Model from second repair.

Figure 5.7: Second repair geometry vs iteration 6 geometry.

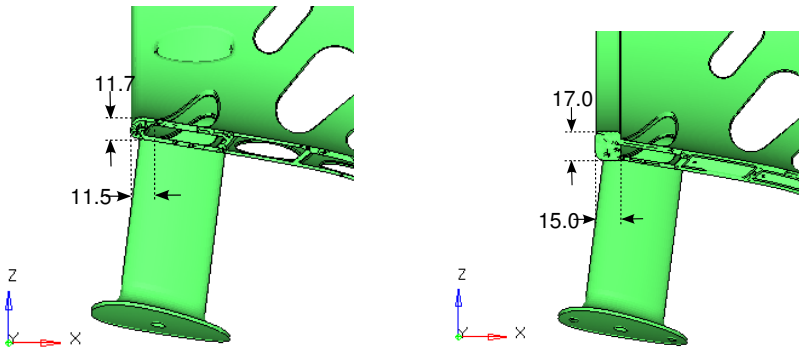


(a) Geometry from iteration 6.

(b) Geometry from second repair.

Figure 5.8: Leading edge section increase with second repair (dimensions in millimeters).

To validate this repairing strategy, a new FEM was created from scratch with the same basic characteristics as the ones from iterations 2 to 6 as demonstrated in table 5.1. Results from this model are displayed on figure 5.9 for the forward load and in figure 5.10 for the rear load case.

From figure 5.9 is clear how drastically the stresses have reduced for the forward load load case. The frontal ring is now absorbing the majority of the load, and since it has such massive section, material plasticity practically doesn't happen.

For the rearward load situation material plasticity still occurs but with the same conditions as iteration 6. So as previously reported in section 4.5 the plasticity levels are acceptable, and this result is

considered acceptable.

| Description | |
|---|---|
| Number of elements | 839 870 |
| Predominant type of element | CTETRA |
| Element size | 1.5mm |
| Roll hoop's weight (from FE model) | 2.91Kg |

Table 5.1: Second repair model characteristics.

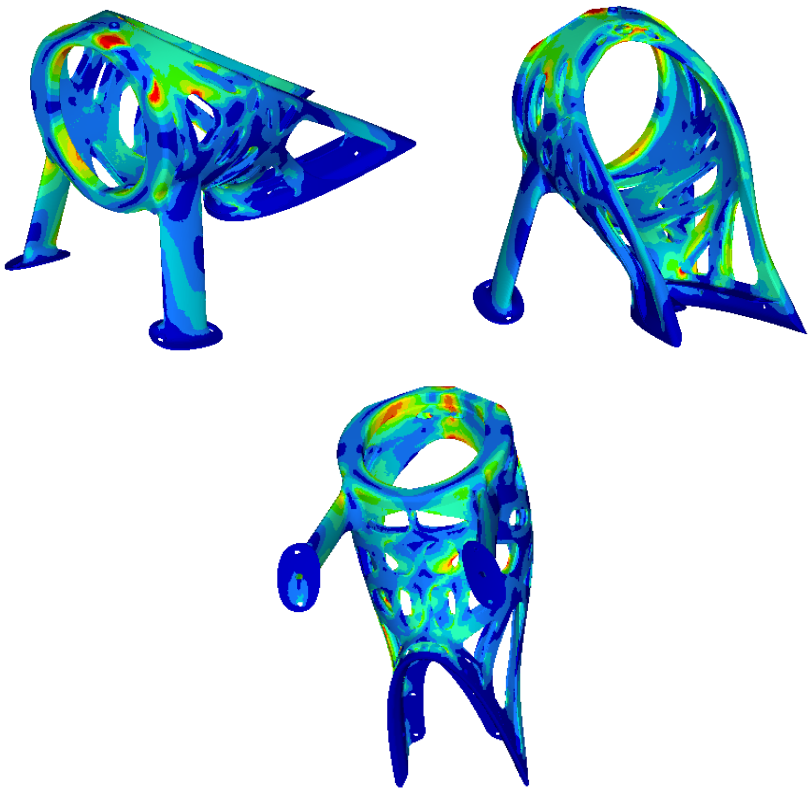

Figure 5.9: Von Mises stress for forward load load case.

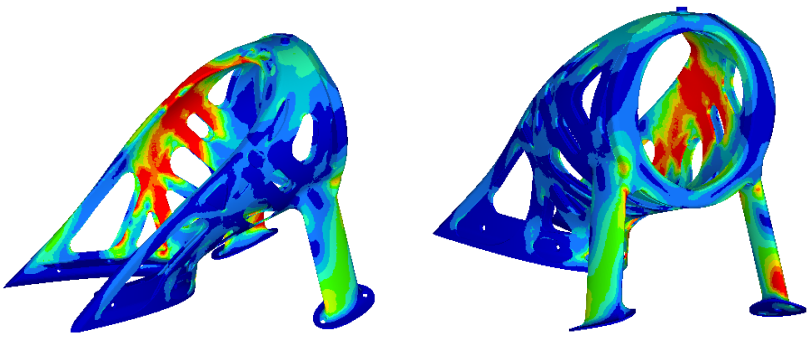

Figure 5.10: Von Mises stress for rearward load load case.

Considering the FEM results here presented it was decided to advance with the repair, and this time the roll hoop was capable of withstanding the 119.2KN load and passed the test. This solution came at

a considerable cost in the weight of the roll hoop, but considering the circumstances it was mandatory to sure that this component passed the required tests. And although the roll hoop increased its mass in 15.9%, it only represents an increase of 0.4Kg in the car weight, which is neglectful when compared with the car's total weight of approximately 800Kg.

# Chapter 6

# Conclusion and Further Work

## 6.1 Conclusion

The focus of this work was to, from a starting point geometry, create the lightest structure possible that could withstand an extremely high load without breaking. This goal has been reached, even though an unfortunate defect alien to this work during the manufacturing process did not allow the prof of this point.

With hindsight the welded patch of the first repair should have never been added since the second roll hoop did not presented manufacturing defects and thus it would be able to withstand the 119KN load. But faced with the original failure it was thought to be better to add a local reinforcement. This was an incorrect call, which has complicated further the supply problems being faced.

Nevertheless, is not only remarkable how competitive this component is considering the short time it took to develop, as is also to stress the cold blood required to take the correct decisions in such sensitive occasions as the ones where the component failed.

Table 6.1 resume the results obtained along this iterative process for a better perspective of the evolution along the iterations.

| | Weight *[Kg]* |
|---|---|
| Iteration 1 | 6.21 |
| Iteration 2 | 2.16 |
| Iteration 3 | 2.47 |
| Iteration 4 | 2.62 |
| Iteration 5 | 2.71 |
| Iteration 6 | 2.51 |
| First repair | 2.52 |
| Second repair | 2.91 |

Table 6.1: Weight evolution along the iterative process.

## 6.2 Achievements

Is important to notice that in this work several engineering stages such as: design, structural sizing, manufacturing and testing have been closely followed. This allows to have very good perception of

how the decisions of each individual stage affects the other. A very important notion to have in the engineering world that can only be learned in practical works such as this.

Also to notice that regardless of how well all the studies are performed, the materialization of a CAD/FEA model from the digital to the real world is absolutely decisive. In other words, when creating something that must be built, one must always consider the manufacturing process and all its constraints. Thus the common motto ”design for manufacture”. Also to account with unpredictable problems, such as the ones found in this project, is prudent to take defensive strategies like using loads higher then the expected or not to account with the material full strength so that the change of success of the project increases. Regardless, in the end is never possible to create a 100% ”bullet prof” design.

Nowadays, the professional world is sadly embedded in a stressful environment where quick answers are mandatory due to time constraints. Since the time schedule to do this optimization was very short, this work also served as learning experience on simplifying problems to deliver quicker but still good results.

## 6.3 Further work

For a further work on this subject it would make sense to evaluate the possibility of changing the initial design domain geometry, since the final repair violated this. This violation might suggest that a simple change in the original geometry could lead even into a lighter and more efficient design without compromising other functionalities.

A further optimization could still be made on the geometry form iteration 6 to remove the final grams of the roll hoop.

In the event of possibly changing the original geometry/design domain, evaluate the possibility of making the roll hoop of cheaper and lighter material such as Aluminium.

# Bibliography


[1] Michell A. G. M., 1904, ”The limit of economy of material in frame structures”, Philosophical Magazine.

[2] Bendsøe M. P., Sigmund O., 2003, ”Topology Optimization. Theory, Methods and Applications”, Springer.

[3] HyperWorks manual, version 10, Altair Engineering.

[4] Abaqus 6.8 manual, Dassault Systèmes

[5] ”2012 FORMULA ONE TECHNICAL REGULATIONS”, Federation Internationale de l’Automobile.

[6] Rozvany G. I. N., 2008, ”A critical review of established methods of structural topology optimization”, Springer.

[7] Bendsøe M. P, 1989, ”Optimal shape design as a material distribution problem”, Structural Optimization.

[8] Bruns T. E., Tortorelli D. A., 2003, ”An element removal and reintroduction strategy for the topology optimization of structures and compliant mechanisms”, John Wiley & Sons, Ltd.

[9] Bruns T. E., Sigmund O., Tortorelli D. A., 2002, ”Numerical methods for the topology optimization of structures that exhibit snap-through”, John Wiley & Sons, Ltd.

[10] Rozvany G. Y. N., Zhou M., Birker T, 1992, ”Generalized shape optimization without homogenization.”, Springer.

[11] ANSYS 12.0 manual, ANSYS Inc.

[12] Hemp W., 1973, ”Optimum structures”, Claredon Press, Oxford.

[13] Rozvany G. I. N., 1989, ”Structural design via optimally criteria”, Kluwer Academic Publishers Group, Dordrecht, Boston, London.

[14] Rozvany G. I. N., 1976, ”Optimal Design of Flexural Systems”, Pergamon Press, Oxford.

[15] Courant R., 1943, ”Variational methods for the solution of problems of equilibrium and vibrations”, Bulletin of the American Mathematical Society.

[16] Hrenikoff A., 1941, ”Solution of Problems in Elasticity by the Framework Method”, Journal of applied mechanics.

[17] Turner M. J., Clough R. W., Martin H. C., and Topp L. J., 1956, ”Stiffness and Deflection Analysis of Complex Structures”, Journal of Aeronautic Science.

[18] Noran Engineering, 2004, ”Accuracy and Performance Comparison NEiNastran vs. MSC.Nastran vs. Abaqus vs. Marc”.

[19] Reddy J. N., 2006, ”An Introduction to the Finite Element Method”, 3rd edition, McGraw-Hill.

[20] Dewirst D. L., and Grinsell P. M., ”The CTETRA(10) Element”, Ford Motor Company.

[21] Kevin Arden E., ”Evalutaion od MSC’s Parabolic Tetrahedron Finite Element”, SEAWOLF Hull Engineering.

[22] Argyris J. H. and Kelsey S., 1955, ”Energy Theorems and Structural Analysis”, Aircraft Engineering.

[23] Clough R. W., 1960, ”The Finite Element Method in Plane Stress Analysis”, Journal of Structures Division.

[24] Parlett B. N., 1980, ”The Symmetric Eigenvalue Problem”, Prentice-Hall.

[25] Newman M., and A. Pipano, 1973, “Fast Modal Extraction in NASTRAN via the FEER Computer Program,” NASA TM X-2893, pp. 485–506.